Geo-information Science and Remote Sensing

Thesis Report GIRS-2023-16

Soil impact of headland turning operations in path-planning for an autonomous tracked vehicle.

Chris Bulthuis

Registration number: 1019061

Date, 2023

Wageningen, The Netherlands

The soil impact of headland turning operations in path planning for autonomous tracked vehicles.

Chris Bulthuis

Registration number 1019061

Supervisors:

dr.ir. S (Sytze) de Bruin
G (Gonzalo) Mier Muñoz, MSc

A thesis submitted in partial fulfilment of the degree of Master of Science
at Wageningen University & Research,
The Netherlands.

Date, 2023
Wageningen, The Netherlands

Thesis code number: GRS-80436
Thesis Report: GIRS-2023-16
Wageningen University & Research
Laboratory of Geo-Information Science and Remote Sensing

Abstract

The introduction of autonomous vehicles in agriculture comes with the need for solutions which are normally performed by the operator of a vehicle. This requires new technology for perception, localization, planning, control, and system management to fully utilize and apply an autonomous solution in practice. Related to the aspects: localization, planning, and control, the Fields2Cover project of Wageningen University is providing a solution for the path planning of unmanned ground vehicles applied in agriculture.

This report introduces new quantification methods about soil compaction and interactions, due to the autonomous vehicle, which are of interest for the stakeholders of the project. In agriculture, soil is the most valuable asset and therefore needs to be handled with care. In this research the soil compaction and the area which the autonomous vehicle drives on (the disturbed rea) are considered. The compaction is quantified by means of the change in bulk density. This is done using the SoilFlex model implemented in the SoilPhysics library available for the programming language R. The methods give an in-depth description of how this model is exploited in this research. Additionally, the methodology for quantifying the disturbed area is explained where a generated path of the Fields2Cover library is used to derive the total disturbed area caused by the trafficking of the vehicle.

The methods were applied on a selection of variations and configurations of model inputs considering the compaction and the disturbed area. It was found that the implemented soil model provided useful insight into the effects the vehicle has on the soil. The modifications making the model applicable for a tracked vehicle were tested and the resulting patterns agree with findings in literature. For the full track system, consisting of the idler wheels and rollers, patterns of the introduced compaction were retrieved based on the load distribution on the track and the resulting bulk densities were analysed.

The disturbed area methodology was applied on a variety of turn variations and other input variables to get insight in the total area covered by the tracks as a result of the turning manoeuvres. Applying the methodology on a field scale allowed for analysis and provided insight on the optimal solution related to the disturbed area for a convex field with an area of 1 hectare. In case of this project it was found that the total disturbed area was minimized when the swath direction was optimized for the total length and a snake pattern was implemented.

The main findings of this research are that the newly introduced quantification methods related to the compaction and the disturbed area provide a useful representation of the effects observed in reality. Analysis related to the compaction and disturbed area, and especially the integration in the software, needs to be researched further to provide a robust product contributing to a ‘farmer ready’, practically integrable solution.

Contents

Table of Abbreviations

Abbreviation	*Description*
BD	Bulk Density [$Mg\ m^{-3}$]
CAD	Computer Aided Design
CI	Compression Index [-]
COR	Centre of Rotation
$COR offset$	The offset of the COR related to the centre of the front idler [mm]
CPP	Coverage Path Planning
CTF	Controlled Traffic Farming
DA	Disturbed Area
DW	Disturbed Width
$F2C$	Field2Cover
fBD	Final Bulk Density [$Mg\ m^{-3}$]
$GNSS$	Global Navigation Satellite System
iBD	Initial Bulk Density [$Mg\ m^{-3}$]
ITE	Individual Track Element
OAT	One at a time
OS	Operating State
pF	Matric Suction
RCL	Recompression Line
RCL'	Steeper Recompression Line
SA	Sensitivity Analysis
TL	Track Load [kg]
TS	Turning State
TW	Track Width [mm]
UGV	Unmanned Ground Vehicle
VCL	Virgin Compression Line
ww	Working Width
YL	Yield Line

1 Introduction

In modern agriculture, technology plays a key role in the day-to-day operations on a farm as a substitution for manual tasks, the execution of decision-making, and for improving the utilization and efficiency of inputs (Rehman et al., 2016). One can think of task maps for variable seeding or applying fertilizer (NPPL, 2019), crop monitoring using drone or satellite imagery for observing plant health (Cuaran & Leon, 2021; Kramer et al., 2015), and climate systems to automate the conditioning within barns for storing crops (Versluis, 2006). These technologies have, since being implemented, been excessively improved on (Tsouros et al., 2019; van der Horst, 2015). As a result, many tasks can be automated to a certain extent which provides a solution for the decrease in available labour in the agricultural sector (European Commission, 2021; International Labour Organization, 2021; U.S. Department of Agriculture, 2022). One aspect that has not really changed since horses were replaced, is that fieldwork on farms is still being performed using operated vehicles, like a tractor or a harvester. In the early 1990s however, guidance based on global navigation satellite systems (GNSS) was introduced easing the operation of tractors by providing a solution for accurate steering. This led to improving the efficiency of operations performed in the field (Brase, 2005). A GNSS guidance system makes the vehicle follow a predefined track or direction (Clemson University, n.d.). This means that overlap between swaths can be significantly reduced and the farmer can be focussed on the controls of the implements (Kharel et al., 2020).

In the practical process of using guidance systems, there is a need to create tracks for each edge of the field to be able to follow the contours of the field utilizing GNSS guidance. For straight sides of a field, a farmer will set a direction or uses two points at the start and end of the field edge. For curving field edges, the farmer logs this curve while driving and the track is generated based on this logged curve. This is a tedious and time-consuming process that will result in lines that are varying based on the operators' preferences and will accordingly, for example, result in a different initial distance to the actual field boundary. These differences must be considered and corrected for in each operation. Besides this, a farmer will most of the time select a straight side of the field for the main direction of operation as this is considered the easiest.

The above process can be facilitated using a solution that generates the tracks for guidance, starting with an arbitrarily shaped field. For this field, a digital boundary is required. This means that a highly detailed mapping of the edge of the field must be made (H-Wodka, n.d.). This provides a significantly better starting point for the generation of tracks compared to what a farmer can manually create by driving over and around the field. One example of automated track generation based on a field boundary is available in VarioGuide. VarioGuide is the guidance and steering system optionally integrated into Fendt tractors (Fendt, n.d.-a). The contour assistant software allows the generation of contour segments and contour tracks (Figure 1). With this tool, a farmer can generate a solution for the coverage of a field based on its boundary.

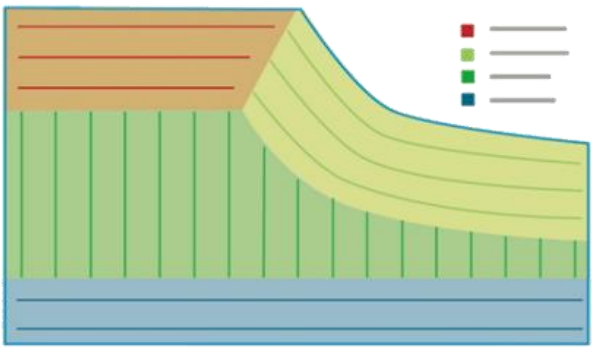

Figure 1: Example of contour segments generated based on the field boundary by the VarioGuide Contour Assistant. Retrieved from:(Fendt, n.d.-a)

The example indicates a shift from the use of individual guidance lines to work the field to considering the shape of the field and defining the guidance lines in such a way the field is optimally covered. The problem faced is a Coverage Path Planning (CPP) problem. This problem is about the objective to fill an arbitrarily shaped area. To do this a path covering the whole area of the shape is determined (Nielsen

et al., 2019). Alternative applications where this problem is introduced are vacuum cleaning robots (Yakoubi & Laskri, 2016). The difference between this application and its use in agriculture is that a cleaning robot needs to cover the area, but it is not required to do this in a way that suits the cultivation of crops. Additionally, overlapping is not a problem in the case of cleaning robots here this might be considered a benefit. Therefore, there are minimal requirements to the paths which the cleaning robot should follow. In contrast for field cultivation practices there are additional requirements related to for example compaction and the consideration of crop cultivation practices (de Bruin, 2020). The paths resulting from solving the CPP problem are of great importance for a manned or unmanned agricultural vehicle to be able to follow this path using its GNSS guidance (Dziuk, 2021).

Since the introduction of GNSS guidance to ease the task of the operator during cultivation, there has been a new development. Autonomy is entering the agricultural scene. The growing interest in Unmanned Ground Vehicles (UGVs) in agriculture raised the need for solutions for the guidance of these vehicles. For UGVs, the process of creating guidance tracks should not have to rely on farmer input. Manufacturers of UGVs have different approaches in terms of scale. Some companies are working on small-scale solutions (Figure 2A), intending to implement swarms (Fendt, n.d.-b; Naio Technologies, n.d.). In the scope of larger-scale robots, it is observed that some manufacturers are trying to modify or tech-up their existing machinery to make these operate autonomously when needed (CHN Industrial, 2017; John Deere, 2022). Lastly, there are newly developed robots meant to replace conventional tractors (AgXeed, n.d.-b).

A B C

Figure 2: Examples of autonomous vehicles. A - Fendt Xaver, B – John Deere 8r modified with sensors (e.g on top of the front weight) to operate autonomously, C – The AgXeed AgBot 5.115T2. Retrieved from: (ducksize.com, n.d.; Fendt, 2020; John Deere, 2022)

To make a vehicle work autonomously, functional elements which are normally performed by the operator must be substituted. Akca et al. (2020) describes five functional components of autonomous vehicles: perception, localization, planning, control, and system management. For an agricultural UGVs, the functional elements mainly relate to controlling the implements, observing the surroundings, and guiding (steering/directing) the vehicle (Shamshiri et al., 2018). The concept of GNSS guidance and related solutions are useful for UGVs as CPP can be performed in advance of a task and solutions can be generated specifically for the scale of the robot.

The need for software to solve the CPP problems related to UGVs is provided by the Fields2Cover (F2C) software library. The F2C project brings forth an open-source software that can provide solutions for the CPP problem by generating the guidance lines to be used by UGVs (de Bruin, 2020; Mier, 2022). In this project, multiple aspects are considered as the software will be utilizing information related to efficiency, kinematic constraints of the machine-implement combinations, soil compaction, conservational practices, and constraints imposed by environmental regulations for its objective functions. Currently, the objective functions consider the field with the headland areas being excluded. Based on the outcome of the objective functions the optimal work direction is determined and accordingly, the swaths are generated.

1.1 Motivation

This project concerns an MSc Thesis as part of my MSc Biosystems Engineering at Wageningen University & Research (WUR). The topic has come forth out of the development of the Fields2Cover (F2C) project which is currently being performed by a member of the GRS faculty at WUR. The project is related to the AgXeed portal for testing purposes. This portal provides a management system for the machinery fleet of a farmer (AgXeed, n.d.-a). This system provides the farmer with a digital environment for planning and managing their farm. Using the F2C library, the planning of field operations and the generation of the optimal swaths the robot must follow to complete a cultivation task can be performed. In the development of the F2C library, the topic of this study is introduced to gain insight into the soil-track interactions during turning operations introduced by the autonomous tracked robot developed by AgXeed. The findings of this study provide insight by the introduction of new quantification methods which has led to the definition of new objectives which could be applied in the optimization of turning operations required to cultivate the fields.

1.2 Problem Description – Current Situation

The introduction describes how farmers use GNSS guidance systems and how the swaths are generated. Based on software solutions available in the present day it is possible to generate the paths improving accuracy and it standardizes aspects that would normally be influenced by personal preferences.

The current functionality of F2C is shown in Figure 3 and gives an overview of the steps involved in the process of generating the solution for the CPP problem. The process consists of four steps. The first step is to import the field boundary (the geofence). Alternatively, a field can be randomly generated as is done in this report/example. Based on the field boundary the headland boundary is generated (Figure 3A). This step is required to provide space for the turning operations to transfer from one swath to another. Secondly, the swaths are generated using one of the objective functions, or if required using a custom angle (Figure 3B).

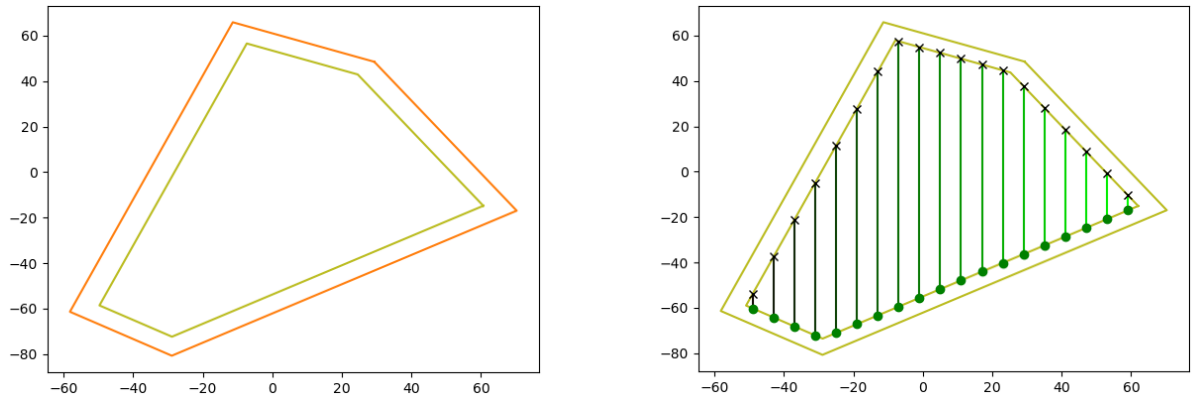

Figure 3: Overview of the processes performed to solve the coverage path planning problem for an arbitrary-shaped field. A – Generation of headlands providing space for the turning operation. B – Generation of the swaths, here done using a custom angle. Retrieved from: (Fields2Cover, 2022a, 2022b)

Accordingly, the route planner is applied. This step determines the order in which the swaths are processed and indicates the start and endpoints of the individual swaths (Figure 4A). The current version of the software has a selection of patterns to do this. Lastly, the start and end points are linked by generating the curve used as the path to follow while executing the turn (Figure 4B). This is done based on a preselected type of curve for which the shortest path is generated.

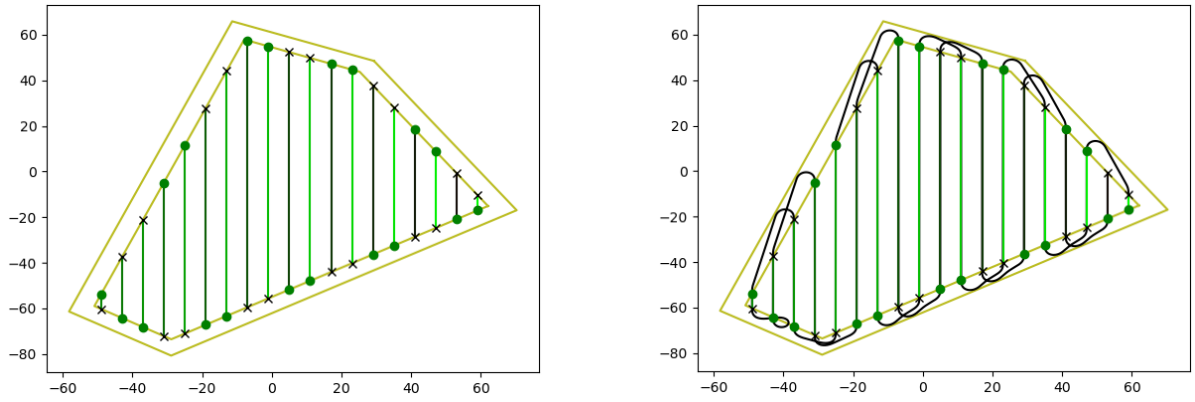

A B

Figure 4: A – The order of the operation is shown from green (first) to black (last) swath, additionally the start (green dot) and endpoints (black cross) are indicated. Here the route planning is done based on snake order. B – Result of the generation of the turning shapes based on Dubins curves with continuous curvature. Retrieved from: (Fields2Cover, 2022c, 2022d)

For the optimization in the software, the step in which the swaths are generated allows for optimization in terms of a cost function. For example, a minimization can be performed on the total length of the swaths or the number of swaths. A cost function is minimized which results in an optimal solution for the given objective. This objective is only applied to the area within the field from which the headlands are excluded. Accordingly, straight swaths are generated. Currently, in terms of the turning of the vehicle on the headlands, no optimization is implemented. The software allows for the selection of turns based on Dubins curves (Dubins, 1957) or the Reeds-Shepp curves (Reeds & Shepp, 1990), for the selected method the shortest possible path is implemented in the solution to get from one swath to another within the field based on the order and the start and end points of the swaths.

1.3 Problem Statement

In terms of the turning operations required to change swaths within a field, it is mandatory to introduce the relevant elements related to kinematic constraints of machine-implement combinations and soil compaction to optimize the path on the headland. This results in minimized influences of the robot on the soil which is better in terms of crop production.

As of now the turn performed on the headlands is generated based on a set radius and minimizing the length of one of the given turn types (Dubins or Reeds-Shepp) (Fields2Cover, 2022d). However, the length of the path is not the only criterion a farmer considers for describing an optimal turn. Here aspects of time and/or compaction play a role. Ultimately, the application of a mix of turn types could provide an optimal solution. Therefore, in this study, the goal is to introduce new quantification methods for the disturbed soil in terms of area and soil compaction.

1.4 Objective

In this project, the focus is on the turning operation executed on headlands. For the turning operation, there are a variety of options related to the shape of the driven path to move from swath to swath resulting from the generated solutions of the F2C software. During the turning operation, several effects play a role on the soil with the main one being soil compaction. The goal is to find the most relevant effects and create a link from these effects to the F2C software. This results in recommendations for optimizing and selecting the most suitable form of turn for the given situation based on the soil state and shape of the field. The findings based on the new quantifications are to be tested and compared on turn and field scale.

1.5 Research Questions

1) What model is suitable for predicting soil compaction created by a tracked vehicle?
2) What manoeuvring aspects of a track-driven vehicle are to be considered for assessing the impact of generated turns?
3) Which model variables incite a sensitive response concerning the compaction and disturbed area quantifications?
4) Which of the currently implemented methods of the F2C library produces the least disturbed area on a selected convex agricultural field using an unmanned ground vehicle?

1.6 Demarcation

The robot used as the vehicle in this project is available in a wide variety of configurations. One of these is selected and used in the models. For this robot two states are defined. One refers to the operation in the field and the other is related to the turning operation. For these states, the Centre Of Rotation (COR) is derived based on a simple approximation. It is assumed that this approximation is suitable for this project but a more elaborated physical model of the robot in combination with the implements is required to find the exact position of the COR. Additionally, related to the load also a simplification applies. It is assumed that both tracks carry the same load. However, in practice, the outer track will be more stressed as a result of the velocity of the robot causing it to loan outward.

One predefined field situation is used. In terms of the geometry of the field, one situation is defined and used for all testing purposes. Additionally, this field has a homogenous soil type which is selected based on its implementation in another research. This makes it possible to compare outcomes if needed. Related to the soil properties and the corresponding variables to be used in the model the same applies, these were retrieved from alternative research on the topic.

The current F2C library provides four methods, including Dubins and Reeds-Shepp variations with and without continuous curvature, for calculating turns. Only the Dubins variations are considered for the for the compaction aspect as this variation does not require a directional change (forward/backward) of the robot. With the Reeds-Shepp variation a directional change is required, and breaking is involved which could result in peak stresses on the soil which is not simulated in this thesis. Additionally, overlap is introduced using Reeds-Shepp which the current implementation of the methods does not account for in terms of the compaction aspect.

2 Theoretical Background

This chapter introduces the background, equations, and framework for the methods later described in this report (section 3). The methods consider the quantification of soil compaction and the disturbed area. First, this chapter will introduce the literature related to soil compaction (section 2.1). Secondly, the soil compaction model used in this project is introduced with a description of the different modules (section 2.2). Next, the pressure distribution of tracked systems is analysed. This provides insight into the approach for modelling soil-track interactions in this project (section 2.3). The soil compaction and disturbed area are related in terms of contact area, this area is defined as the contact area the track or wheel of an UGV has with the soil. Therefore, the soil-track interactions in a spatial context are also introduced (section 2.4).

2.1 Soil compaction

For the compaction, the weight distributed over the contact area is needed to assess the effects of a pass of the UGV has on the soil. For this project, the soil compaction is expressed as the soil deformation which is quantified through the change in bulk density (BD) expressed as $Mg\ m^{-3}$ of the soil. Buckman and Brady (1960) described the BD as the mass of the particles of the material divided by the total volume (including the particle volume, inter-particle void volume, and internal pore volume) they occupy. The calculations required to determine the BD are based on the Critical State Theory as suggested by O'Sullivan and Robertson (1996).

$$BD = \frac{\rho_{solid}}{v} \tag{1}$$

Equation 1 provides the calculation of the bulk density from the specific volume (v [-]) and soil density (ρ_{solid} $[Mg\ m^{-3}]$) (O'Sullivan & Robertson, 1996). This equation provides insight into the volume variations of soil and is used to compute the relations in the terms of the soil compression curve. The specific volumes used to determine the final BD (fBD) of the layers are determined by the region of the $v - \ln(\rho)$ space (Figure 5).

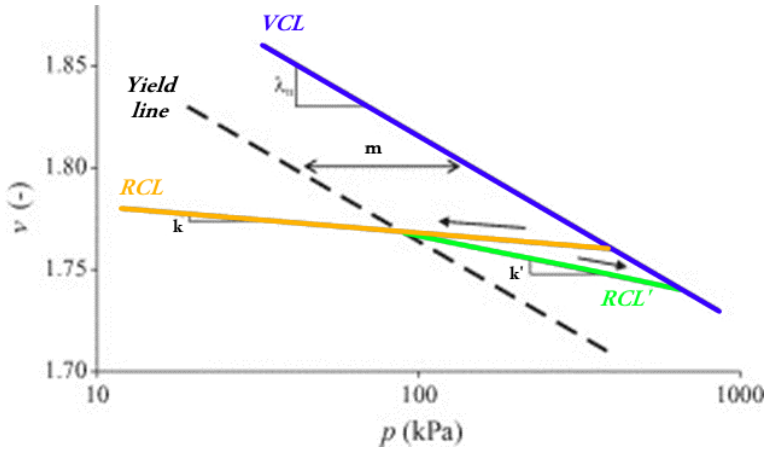

Figure 5: Model of rebound and recompression in terms of the specific volume and mean normal stress, p. VCL: virgin compression line; RCL: recompression line; RCL': steeper recompression line; λn: compression index; κ: recompression index; κ': the slope of the steeper recompression line; m: value that separates the yield line and the virgin compression line. Retrieved and modified from: (de Lima, da Silva, et al., 2021)

The decreases in specific volume (v) as a function of the normal stress (p) is found following the line corresponding to the equation relevant for each region (Figure 5). The starting point is at the left of the RCL. The RCL is followed till the intersection with the Yield Line. Then the RCL' is followed and eventually the last region is described by the VCL in the bottom right corner. The specific volume for each region was calculated using the formulas, equations 2, 3 and 4, as defined by O'Sullivan and Robertson (1996).

First, the VCL is calculated to find the initial specific volume (v_{init}). This requires N, which is the specific volume at $p = 1kPa$ [-]. Accordingly the RCL and RCL' are calculated.

$$VCL: v = N - CI * ln\,(p) \quad (2)$$

$$RCL: v = v_{init} - k * ln\,(p) \quad (3)$$

$$RCL': v = v_{yield} - k' * ln\,(p) \quad (4)$$

Where p stands for the mean normal stress [kPa], CI is the compression index, kappa (k) is the recompression index, k' is the steeper compression index. CI, k, and k' are based on soil properties and are calculated by methods described by (de Lima et al., 2018; O'Sullivan & Robertson, 1996).

Using the process of deriving the specific volume to calculate the BD as a result of an applied stress provides a way of determining soil compaction. This is achieved by assessing the change in BD.

2.2 Soil compaction model

The description of soil compaction using the change in BD is applied in models simulating the resulting BD as a result of an applied stress. Keller et al. (2007) describes such a soil compaction model, *SoilFlex*, which was created by combining aspects of a variety of other compaction models (O'Sullivan et al., 1999; Söhne, 1953; Van den Akker, 2004). On request, this model is available as an excel document. There is also a publicly available software library for the programming language R, called *soilPhysics* (de Lima, da Silva, et al., 2021). This library contains a set of functions performing the simulations and calculations resulting in useful aspects for this project and is eventually able to calculate the BD state. Firstly, the stress exerted on the soil, resulting from the applied load, is estimated for a set of soil layers. This gives insight into the stress distribution in the soil below the contact area of a wheel in the case of the original *SoilFlex* model. Next, the resulting BD was quantified from the stress distribution matrix. This process is performed in the following modules: *stressTraffic* (section 2.2.1), *soilDeformation* (section 2.2.3), and *compresiveProperties* (section 2.2.2) (de Lima & da Silva, 2021a, 2021b).

2.2.1 Soil Stress Matrix

The *stressTraffic* module from the *soilPhysics* library for R (de Lima, da Silva, et al., 2021) calculates the stress matrix indicating the mean measuring area stress (p [kPa]) introduced by a wheel . The area stress, p, is calculated using the stress components (σ [kPa]) in x-, y- and z- direction (Equation 5). The individual stress components are calculated for 0.01 by 0.01 metre areas based on the discretised total contact area (A) using a methodology proposed by Keller et al. (2007).

$$p = \frac{(\sigma_x + \sigma_y + \sigma_z)}{3} \quad (5)$$

$$\sigma_z = \frac{F}{A} \quad (6)$$

$$A = b \int_0^a \left(a - \frac{x^n}{y^n}\right)^{\frac{1}{n}} dx \quad (7)$$

$$x = A_l = 0.47 + 0.11 * D_{tyre}^2 - 0.16 * ln\,(\frac{P_{actual}}{P_{recommended}}) \quad (8)$$

The simple representation of the stress of the z- component is calculated by dividing the applied force (F [n]) by the area (A [m^2]) to which this force is applied (Equation 6). This is done for all areas resulting from the discretisation for the total area which, in this case, is described by a 'super-ellipse' shape (Keller, 2005). The area of a super-ellipse is calculated using equation 7 (Keller, 2005; Teimourlou & Taghavifar, 2015). It is described by the width of the tire (b [m]), the contact length (a [m]) and the dimensionless shape exponent (n [$-$]). This equation uses a range based on the tire

width (y $[m]$) and length ($x = A_l$ [m]) as inputs for the integration. The implementation of the super-ellipse area in the original library module requires the tire length (A_{lenght} $[m]$) which is based on the tire diameter (D_{tyre} $[m]$), inflation pressure (P_{actual} $[kPa]$) and recommend inflation pressure ($P_{recommended}$ $[kPa]$) (Equation 8).

2.2.1.1 Soil Stress Matrix for Tracks

The application of the equations above does not suit the case of a tracked vehicle. Therefore, alternative formulas for equations 7 and 8 are implemented. The changes required consider the contact area, which is not related to an inflation pressure for a tracked system, and additionally the stress exertion through the soil is found to be different. Keller and Arvidsson (2016) researched the vertical stress distribution near the soil surface below rubber-tracked undercarriage systems fitted on agricultural vehicles. In this study, the track-soil interface is described as a rectangular shape defined by the contact width (W_c $[m]$) and contact length (L_c $[m]$) resulting in the contact Area (A_{track} $[m^2]$):

$$A_{track} = W_c * L_c \tag{9}$$

The paper also describes alternative equations for calculating the stress component in the *x*- and *y*-direction. Assessing these equations has led to the identification of two mistakes (de Bruin, 2022). The modified versions and a description of the changes are listed below.

$$\sigma(x) = \left(\frac{\sigma_{max}}{2}\right) * \left[cos\left(\left(\frac{2x}{L_r}\right) * \pi\right) + 1\right] \tag{10}$$

$$\sigma(y) = \frac{\sigma_{max}}{a} + \left[\frac{\left(|y| - \frac{W_c}{2}\right)}{\frac{W_c}{2}} * \frac{1-a}{a} * \sigma_{max}\right] \tag{11}$$

Where, σ_{max} is the maximum vertical stress under the axle $[kPa]$; L_r is the dynamic contact length $[m]$; x is the *x*-coordinate of the dynamic length of the track element (idler or roller) taking on values between $-L_r/2$ and $L_r/2$ with a step size of 0.01 metre related to the discretization for the area; y is the absolute width of the track and a is the *y*-coordinate of the width taking on values between $-W/2$ and $W/2$ with a step size of 0.01 metre related to the discretization for the area. In the case of equation 10, π was originally divided by 2. However, this division of two is already accounted for by the division by two in the term $\sigma_{max}/2$. For equation 11 the first term originally was $1/a$, but it was found that it should also contain σ_{max}.

For the component in the z-direction (σ_z), the same method for calculating the vertical soil stress is implemented as was done in the original version of the *stressTraffic* module of *SoilFlex* using (Equation 5). Comparing the model with field measurements, Keller and Arvidsson (2016) concluded that, up to a depth of 0.5 metres, the wheels and rollers were identified as the causes of the peak stresses. At a depth of 1 metre, the stress distribution has a maximum at the centre of the track length.

2.2.2 Soil Properties

For further calculations using the soilPhysics library, the state of the soil needs to be defined. The *compressiveProperties* modules allow for calculating the required variables used for defining the soil situation. Depending on the selected soil type and methodology, the specific volume at $p = 1\ kPa$ (N), CI, and k are calculated (de Lima, da Silva, et al., 2021). The original module provides five versions for calculating the soil state variables. All methods are substantiated by papers that provide the derivation of the formulas (de Lima et al., 2018; de Lima, Rolim, et al., 2021; Defossez & Richard, 2002; Keller & Arvidsson, 2007; O'Sullivan et al., 1999). The empirical formulas are based on field measurements and regression models. The calculated variables provide the properties of the soil providing the information to perform calculations on changes in the soil state.

The specific properties of wet Sandy Clay Loam soil, the soil type selected for this project, are provided in section 3.4 where the field situation is illustrated and explained. These parameters are used to derive the compressive properties of the given soil type. N, CI, and k are calculated using the pedotransfer functions described in equations 12, 13, and 14 following from de Lima et al. (2018):

$$N = 4.036 - 1.727BD + 0.521pF - 0.1pF^2 \quad (12)$$

$$CI = 0.137 - 0.158BD + 0.150pF - 0.029pF \quad (13)$$

$$k = 0.051 - 0.052BD + 0.031pF - 0.006pF^2 \quad (14)$$

Where BD is the bulk density $[Mg\ m^{-3}]$ and pF is the matric suction $[kPA]$

The compressive properties of the soil are used in the soil deformation module to determine the new state of the bulk density for the given soil type and state. For changing the state of the soil in terms of wetness the pF value was changed to simulate a wet or dry situation.

2.2.3 Soil Deformation

This module calculates the change in soil state expressed by the final bulk density (fBD) after the stress has been applied as described in (section 2.1). It considers the soil state and properties (previous paragraph). The input requirements of this module are the stress pattern represented by the stress matrix resulting from the *stressTraffic* module. Additionally, the following information related to the soil is implemented (de Lima, da Silva, et al., 2021): the particle density, *iBD*, *N*, *CI*, *k*, the slope of the steeper compression line (k'), and the value that separates the yield line and the virgin compression line (m) = 1.3, visible in Figure 5 (O'Sullivan & Robertson, 1996).

2.3 Pressure Distribution

The distribution of a load over the track is expected to influence the way a track interacts with the soil. It is expected that a higher load results in a larger stress which is related to a higher pressure (Equation 6). As was described in section 2.2.1.1, the pressure distribution of a track system at relatively shallow depths clearly shows the peak stresses located at the positions of the idlers and rollers (Keller & Arvidsson, 2016). The outcome of this behaviour experienced in their research is shown in Figure 6A. Similar patterns (Figure 6 B&C) have been found in alternative research (Ding et al., 2022; Liu & Cheng, 2020; Liu et al., 2018; Wong & Huang, 2008).

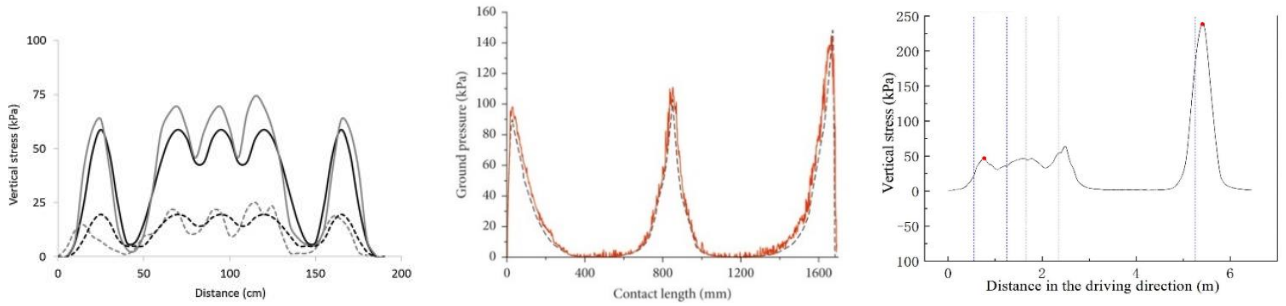

A B C

Figure 6: Examples of stress patterns below tracks. A – Stress pattern associated with a track of a CaseIH Quadtrack. The black line indicates the simulated distribution, and the grey line indicates the measured distribution. Retrieved and modified from: (Keller & Arvidsson, 2016). B – Measured (red line) and simulated (dashed line) ground pressure distribution of a tracked vehicle on soft ground. Retrieved and modified from: (Liu & Cheng, 2020). C – Stress distribution of a Claas Lexion combine equipped with the Claas terratrac system on the front axle (peak pattern on the left) and a wheel on the rear axle (left peak). Retrieved and modified from: (Ding et al., 2022)

Stress patterns as shown above are the result of the exerted stresses by the Individual Track Elements (ITEs), which are the idlers and rollers (wheels) of the track. This means each Individual Track Element (ITE) caries part of the total load of the vehicle. For implementation into the *SoilPhysics* model, the load exerted on each individual idler and roller needs to be determined. One approach would be to assume a uniform distribution. However, a study by Dobretsov et al. (2021) suggests using a distribution where the load increases from the first point of contact the track has with the soil to the end of the track. This effect is expressed in Figure 7 A&B. The effect of the load being distributed more towards the rear end of the robot is especially expected to happen during a turning operation on the headlands. This is explained by the raising of the implement introducing an increased load and a change in the centre of rotation. Both, the change in centre of mass, related to the paths of the individual track elements, and the resulting pressure distribution related to the stress of the individual track elements, are of interest for the research of this report.

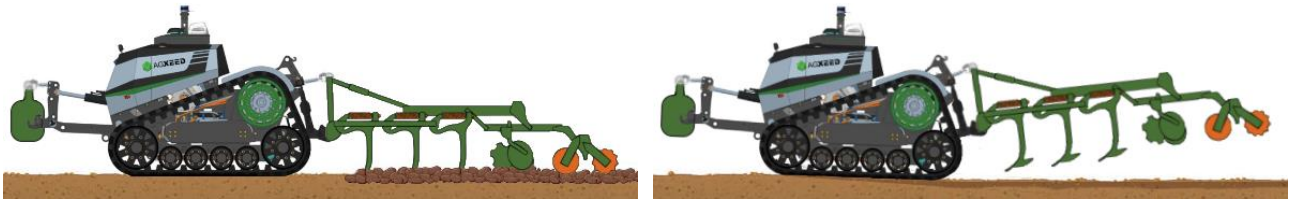

A B

Figure 7: A – The AgBot in working position. The track has a uniform distribution on the soil and the load related to the implement is not relevant. B – The Agbot in transport position as would be the case on headlands. Due to the load of the lifted implement, 'back hang' is introduced which causes a larger stress on the rear end of the track expecting to cause more compaction. Source images retrieved from: (AgXeed, n.d.-a, n.d.-b)

2.4 Spatial Soil-Track Interactions

The spatial part of this thesis research is linked to the path set out for the robot to follow or the path the robot has actually followed based on GNSS tracking. The generated paths use one of the selected methods of the F2C library for the turning operation: Dubins or Reeds-Shepp (Figure 8 A&B). Or their respective continuous curvature variations. The path set out for the robot does however not give any direct insight into the location where the vehicle interacts with the soil. It only provides the path the vehicle attempts to follow based on its guidance steering.

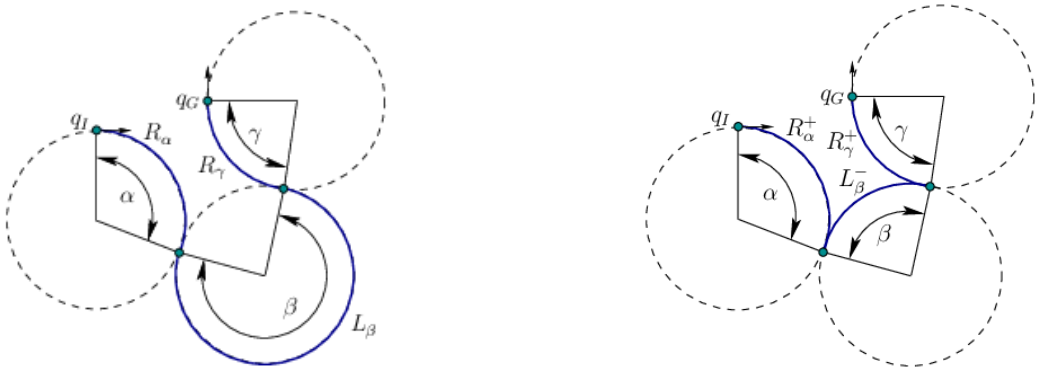

A B

Figure 8: A –Dubins curve: the example shows a Right, Left, Right (RLR) turn configuration resulting in the shortest path from q_I to q_G. B – Reeds-Shepp curve in the same configuration as A. Here is shown that by allowing reversing the total travelled distance is reduced. This situation shows a forward right, backward left, forward right ($R^+L^-R^+$) turn configuration. Retrieved from: (LaValle, 2020a, 2020b)

The interaction of the tracks with the soil during the execution of turns results in skidding of the tracks. Skidding is the sliding of a track as a result of its large contact area. Li et al. (2007) describes a method that provides a way of quantifying the amount of skidding. In his research, an analytical model for calculating the disturbed width (DW) is introduced. The disturbed width is defined as the terrain impact caused by tracked vehicles in the horizontal plane. This model is one of the few models providing a method for calculating the effects of a track on the soil. However, for the purpose of this project, it does not provide the spatial information to perform an analysis which also includes the soil compaction. For this project, an adaptation of the concept by (Li et al., 2007) is introduced (section 3.6.2). The goal is to get insight into the area disturbed during the turning operation performed by the AV. So instead of computing the disturbed width, the disturbed area is considered. The purpose of the disturbed width model could be introduced as a method of validation by comparing the disturbed width with the maximum width the track disturbs based on the calculated area. Concluding, the method of Li et al. (2007) inspired the method implemented in this thesis research.

3 Methods and Data

In this research, the track is approached through at the ITEs. The reasoning for this approach is explained in the next section as this implementation will form the guideline for the other methods introduced in this chapter. The second part of this chapter explains the implementation of the soil model by Keller (2005) with the modifications for a track system related to the code written for this project. Next, the main section of this research will follow where the new quantification methods related to the compaction and disturbed area are introduced. Here the states of the robot are explained which are then used in the determination of the compaction after a full track system has past the soil at a certain point. Furthermore, this involves the deduction of a model for determining the disturbed area based on the path, field, and vehicle properties. These new models are analysed based on a sensitivity analysis. The approach of this analysis is explained in section 3.8. Lastly, the methodology of testing and implementing the findings of this project on a field scale will be explained.

3.1 Individual Track Elements

The stress patterns shown in section 2.3 indicate that the vertical stress or ground pressure below the track is mainly present at the place where the idlers and rollers have contact with the track and therefore indirectly with the soil. The idlers are the large front and rear wheels of the track, and the rollers are the smaller wheels in between (Figure 7). Based on published research, discussed in section 2.3, it was concluded that the expressed stresses are significantly more apparent below the ITEs compared to the area where the track is not supported by one of these elements. Therefore, it was decided to not consider the full track as a whole. Alternatively, the ITEs are considered in a component-wise manner. This means that for the AgBot used in this research a total of 6 wheels are modelled. The two idlers and four rollers are considered individual parts of each track. The physical dimensions (width and diameter) and the location of the individual elements are used for determining the effects on the soil.

Originally, the *soilPhysics* model is solely suited and used for wheeled vehicles. The influence of a single wheel on the soil is quantified using the applied stress and physical size of the wheel which leads to an increase in the bulk density. The functioning of the model solely for wheels is confirmed by inspecting the input variables and the equations for determining the soil stress of the modules. Assuming that each element of a track behaves similarly to a single wheel allows for the application of SoilFlex. This approach is explained in section (3.2).

Concluding, the decision to consider the track using the ITEs makes the use of the *soilPhysics* model possible which allows for the assessment of the compaction by the track. Additionally, a starting point for generating a methodology for assessing the disturbed soil based on the passing of the AgBot is set.

3.2 Implementation of the Modified Soil Model

The *soilPhysics* library provides the modules for calculating a stress matrix, the compressive properties, and the resulting bulk density (fBD). The original library is made for the programming language R (n.d.). However, the coding language selected for this research is Python (n.d). Specifically, Python version 3.7 is used. To be able to use the R library modules (*stressTraffic* and *soilDeformation*), these modules were bridged to Python using the r2py (n.d.) library. This library provides the possibility to define console commands in Python as if the code was run in R. The rpy2 library (r2py, n.d.) runs this code within an R kernel and returns the resulting output to the python environment. The *compressiveProperties* module was rewritten in Python as this module was easier to rewrite as it did only involve standard computational operators (multiplication, division, etc.)

A total of four Python scripts was prepared for the implementation of the soil model:

- *stressTraffic.py*, bridge to the *stressTraffic* module of the *soilPhysics* library in R.
- *stressTrackedTraffic.py*, bridge to *stressTrackedTraffic.R* which is a modified version of the original *stressTraffic* module with changes as suggested in section 2.2.1.1.
- *compressiveProperties.py*, rewritten version of the original module.
- *soilDeformation.py*, bridge to the *soilDeformation* module of the *soilPhysics* library in R.

The coherence between these four scripts shown in Figure 9. This flowchart gives an overview of how the required inputs and outputs of the individual *soilPhysics* modules are linked resulting in an overview of the implementation of the modified soil model.

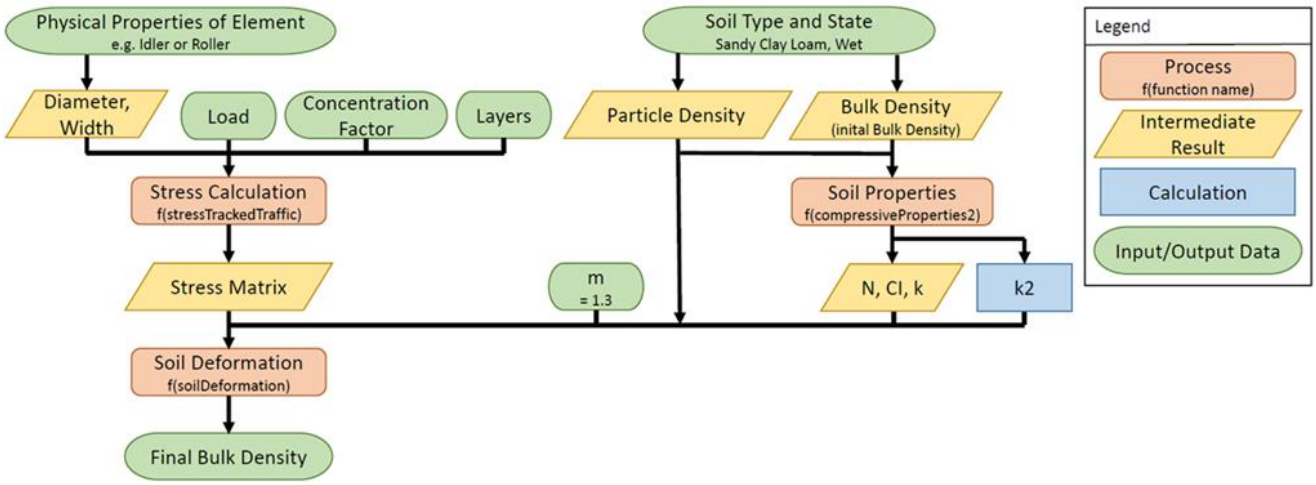

Figure 9: Flowchart of the steps and flows of data through the soilPhysics library functions used for this project.

Using the *stressTraffic* or *stressTrackedTraffic* module generates a stress matrix for an individual wheel or track element by providing it with the following input variables related to the vehicle:

stressTraffic

- Tire width [m]
- Tire diameter [m]
- Wheel load [kg]
- Inflation pressure [kPa]
- Recommended inflation pressure [kPA]

stressTrackedTraffic:

- Contact Width [m]
- Dynamic length [m]
- Load [kg]

Additionally, a list of soil layers in terms of depth [m] is required to provide the model with the information at which depths the simulation needs to be executed. Lastly, related to the individual soil layers the corresponding concentration factor needs to be provided. These are related to the water content in each layer and have a value between 3 (saturated soil) and 6 (dry soil) (de Lima, da Silva, et al., 2021). For this research, the soil layers were split at 0.05, 0.1, 0.3, 0.5, 0.7, and 1 metre with the corresponding fixed concentrations factors: 4, 5, 5, 5, 5, 5 [-]. These values are selected considering alternative research (Amsing, 2021; de Lima, da Silva, et al., 2021).

The *compressiveProperties* module is used for calculating additional soil properties. For this project, Sandy Clay Loam in a wet state is used as the standard situation. The *compressiveProperties* module requires the BD and particle density as inputs and returns N, CI, and $kappa$. Lastly, the *soilDeformation* module is implemented which uses the stress matrix and soil properties to calculate the new state of the bulk density after the given stress is applied to the given soil situation.

3.3 Field Robot and Implements

3.3.1 AgBot 5.115T2

The implementation of the method described above requires a selection of input variables pertaining to the used vehicles. In the case of this project, a tracked robot developed by AgXeed is used (Figure 2B). The specific robot is the AgBot 5.115T2. A variety of configurations of the tracks is available for this robot. The differentiation between configurations is based on the track width and the tread width. Appendix D provides an overview of all possible configurations of the robot. For this project, one of these configurations is selected and is used as the 'standard' situation (Figure 10). Table 1 provides the technical data related to this version of the AgBot.

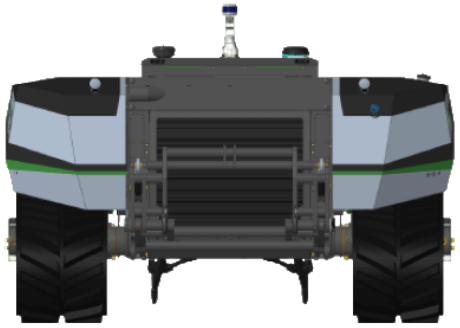

Figure 10: Front view of the AgXeed Agbot 5.115T2 showing the track configuration selected for this project. The track has a stance of 2.25 m and both are 0.61 m wide. Image retrieved from:(AgXeed, n.d.-a)

Table 1: Properties of the AgXeed AgBot 5.115T2. The values are retrieved ([a]) from (AgXeed, n.d.-a) or are estimated using pixel analysis ([b]) (Appendix B). The values are confirmed using the CAD model of the robot.

Property	*Value*	*Unit*
Total Weight (W_r)	7800[a]	$[kg]$
Track Load (TL_r)	3900[a]	$[kg]$
Track Length	2.550[b, 1] (2050[b, 2])	$[m]$
Tread Width	0.610[a] (510[3])	$[m]$
Track Width (TW)	2.250[a]	$[m]$
Idlers (i_n)	2[a]	# per track
Idler Radius	0.550[b]	$[m]$
Rollers (r_n)	4[a]	# per track
Roller Radius	0.300[b]	$[m]$

[1] Based on Appendix C. Contains a deviation with the actual track length contacting the ground as this value is based on the front and end of the track instead of the actual initial and final contact point of the track to the soil.

[2] The corrected value for the length of the track providing a closer representation of the actual track length. It is calculated by subtracting the diameter of the Idler from the original value and additionally considering the concept of the dynamic length of individual track elements as suggested by Keller and Arvidsson (2016). This value is used in the models during the execution of this project.

[3] The actual track width is typically smaller than the nominal track width stated by the manufacturer. This is the result of lug positioning on the track. Therefore, Keller and Arvidsson (2016) suggest subtracting 0.1 m from the track width specified by the manufacturer. This correction is implemented in the calculation of the stress of the *stressTrackedTraffic* module (section 3.2).

3.3.2 Implements: Amazone Cenius and Counterweight.

To simulate a real-life situation, the experiment in this study assumes that the AgBot is equipped with an implement in the rear and a counterweight in the front. The implement chosen is the Amazone Cenius cultivator (Figure 11) which is used in actual field tests and shown in press material of the AgBot being used in the field (AgXeed, n.d.-b).

Figure 11: Amazone Cenius cultivator. Retrieved from: (AMAZONE, n.d.-a)

The properties of the cultivator and the weight are listed in Table 2 and Table 3. The weight of both implements was used in the quantification of the soil compaction. The working width of the cultivator was used for the generation of paths and the physical length is used to approximate the centre of gravity which, related to the weight of the cultivator, is used for defining the vehicle states during the turning operation.

Table 2: Properties of the Amazone Cenius cultivator. Data retrieved from: (AMAZONE, n.d.-b)

Property	*Value*	*Unit*
Total Weight (W_i)	2024	$[kg]$
Working Width (ww)	3	[m]
Physical Length	4.470	[m]

Table 3: Properties of the counterweight.

Property	*Value*	*Unit*
Total Weight (W_w)	500	$[kg]$

3.3.3 Vehicle States

Section 2.3 briefly referred to the two states the robot can have related to this project. In this section, both states are described in more detail and the derivation of the required parameters for the application in the code is given. The two states are referred to as the Operation State (OS), which means the robot is performing the cultivation in the field with a lowered implement. Secondly, there is the Turning State (TS), here the implement is lifted which allows for performing a turn. The effects considered in this project are the location of the COR of the robot. This location is used for calculations of the position of the ITEs relative to the path (section 3.6.2) and also corresponds with the centre of mass of the robot which relates to the distribution of the load on the tracks.

3.3.3.1 Operation State

During operation, the physical relation of the robot and implement is described as follows: The implement is lowered during operation. The forces resulting from this are assumed to be negligible as the counterweight cancels these effects. Therefore, it is assumed that during operation the robot is well balanced, resulting in the COR being located exactly in the middle of the track (Figure 12) and that the

load on the track is uniformly distributed. This uniform distribution of the load results in the total load on the track being equally distributed among the ITEs. In terms of the total load, the weight of the robot and twice the counterweight are considered: $W_{tot} = 2 * W_w + W_r = 2 * 500 + 7800 = 8800\ kg$. The $COR_{offset,work} = 925mm$ which is derived from the position of the ITEs (Appendix B)

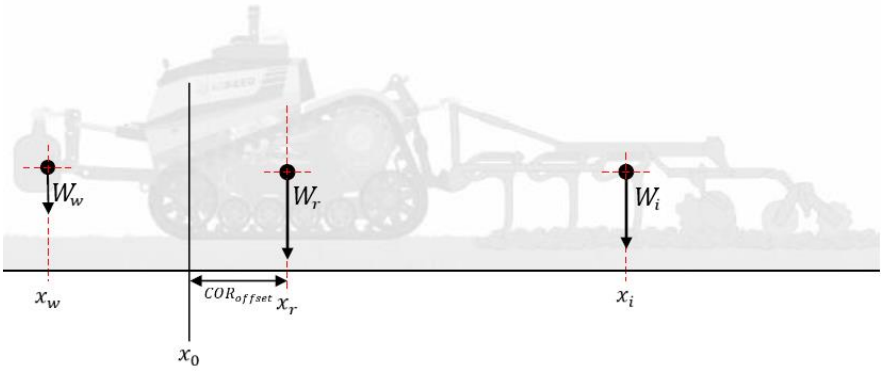

Figure 12: Simple representation of the weights of the individual elements. Additionally, the COR_{offset} is given indicating the distance from the COR (x_r) to the centre of the first idler (x_0) on the x-axis.

3.3.3.2 Turning State

Figure 13 shows the changes compared to the OS. As a result of lifting the implement, a larger load is now applied to the tracks. Additionally, a shift in the centre of mass has occurred changing the COR. The position of the COR is calculated using the weight of the weight (W_w), the robot (W_r), and the implement (W_i) and the relative distance of each centre of mass (Equation 15). The total load on the tracks in this state equals $W_{tot,turn} = W_w + W_r + W_i = 500 + 7800 + 2024 = 10324\ kg$.

$$COR_{offset,turn} = \frac{W_w}{W_{tot,turn}} * rd_w + \frac{W_r}{W_{tot,turn}} * COM_{offset,work} + \frac{W_i}{W_{tot,turn}} * rd_i \qquad (15)$$

$$= \frac{500}{10324} * -685 \ + \frac{7800}{10324} * 925 \qquad + \frac{2024}{10324} * 4730$$

$$= 1593\ mm$$

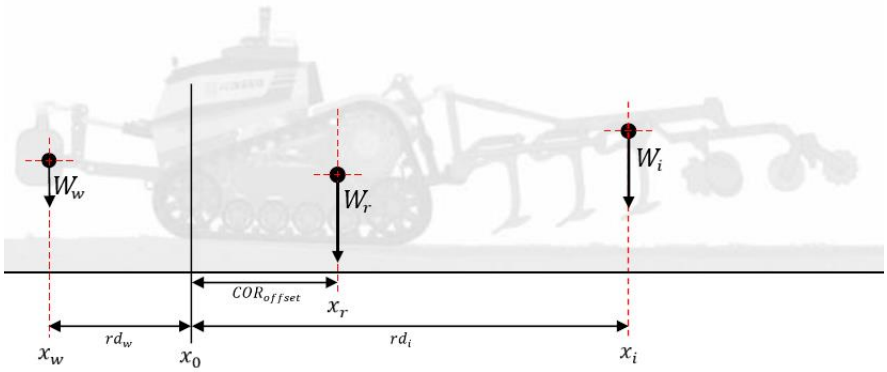

Figure 13: A simplified representation of the weights of the equipment and additionally the relative distances (rd_w, rd_i) between them are indicated which are used for calculating the COR_{offset} for the turning state.

3.3.3.3 Turn State Pressure Distributions

For the pressure distribution on the soil, two additional situations (next to the uniform distribution) are considered in this research. Initially, video footage of the robot was researched to determine the contact of the track with the soil. This led to the definition of a custom weight distribution (Figure 14A). Appendix B contains the calculations for the fractions shown in Table 4. Considering research on the pressure distribution a paper has been found which indicates a one variant where the pressure increases toward the end of the track (Wong et al., 2019). The pressure distribution described by Wong et al. (2019) is implemented in this project and is as defined as the custom distribution. Further investigation has led to the implementation of an alternative distribution. Keller and Arvidsson (2016) have found that, especially in deeper soil layers, the stress distribution has a triangular shape. Using their findings, a triangular distribution is also defined (Figure 14B).

A B

Figure 14: A – Load distribution as described by Wong et al. (2019) and as observed in video footage. B – Visualization of the load distribution as described by (Keller & Arvidsson, 2016).

The load distributions described above were defined as fractions of the total load on the track for each ITE (Table 4). A minimal fraction of 0.05 was set as a requirement for the start and end point in the triangular distribution as it is assumed that both idlers have ground contact and accordingly cause stress on the soil. The reason for considering each ITE was explained in section 3.1.

Table 4: Fractions used for calculating the load on the individual track elements.

	i_1	r_1	r_2	r_3	r_4	i_2
Uniform	1/6	1/6	1/6	1/6	1/6	1/6
Custom	0.016…	0.086...	0.139…	0.192…	0.245…	0.319…
Triangular	0.05	0.102…	0.184…	0.265…	0.347…	0.05

3.4 Soil Properties

In the current thesis research, the soil state is set for an artificially generated convex field which is used for testing purposes.

For establishing a list of soil properties, the needs of the used soil model have been investigated (section 2.2). The soil type selected for this project is a "Sandy Clay Loam" as defined by de Lima et al. (2018). A moist state of the soil was selected to be able to see the largest influences of the vehicle in terms of changes in the bulk density. Alternative soil types such as Sandy Loam and Clay Loam defined by O'Sullivan and Robertson (1996), or Sandy Loam defined by de Lima et al. (2018), and the soil state: moist or dry, was selected and tested for as well. These differences were used in the sensitivity analysis (section 4.3). An overview of values for the Sandy Clay Loam soil properties is given in Table 5. The two variables applied in the models are the iBD and the particle density. The soil the pF value is related to the amount of water present in the soil. The pF value for the moist conditions was set to 2.5; for the dry alternative the pF was set to 3.5. These values were selected in correspondence with research performed by Amsing (2021). Table 6 provides the parameter values related to the soil state properties of a wet scenario.

Table 5: Properties of Sandy Clay Loam soil. Data retrieved from: (de Lima et al., 2018)

Property	*Value*	*Unit*
Clay content	320	$[g\ kg^{-1}]$
Silt content	130	$[g\ kg^{-1}]$
Sand content	550	$[g\ kg^{-1}]$
Initial Bulk Density (iBD)	1.37[1]	$[Mg\ m^{-1}]$
Particle Density	2.65	$[Mg\ m^{-1}]$
SOC	40	$[g\ kg^{-1}]$

[1] Value derived using Saxton equations (Saxton & Rawls, 2006).

Table 6: Soil state-related properties. Data retrieved from: (de Lima et al., 2018)

Property	*Value*	*Unit*
Water content	27.92[1]	$[g_{water}\ g^{-1}_{dried\ soil}]$
Matric suction (pF)	316	$[kPA]$

[1] Value derived using Saxton equations (Saxton & Rawls, 2006).

3.5 Modelling Compaction

Till this point, the new bulk density computation only considers the passing of one single ITE. To simulate a pass of the full track system, a function running through the ITEs and consecutively looping through the other functions was written. It follows the approach of Keller and Arvidsson (2016) and is implemented in the function *simulatePass*, which is part of *soilpass.py*. The script is provided with the vehicle properties representing the information on the ITEs. Additionally, the load distribution method is selected, and the soil-related variables are provided. The *simulatePass* function either simulates the passing of a full track system or that of a selection of the track elements. The latter is relevant for coupling the spatial information that will be introduced in section 3.7. The code simulating the passing of a vehicle is similar to the way Amsing (2021) approached it. Figure 15 shows the flow of data and the steps involved in the *simulatePass* function. Additionally, this flowchart summarizes the calculation of the soil compaction according to the resulting fBD values.

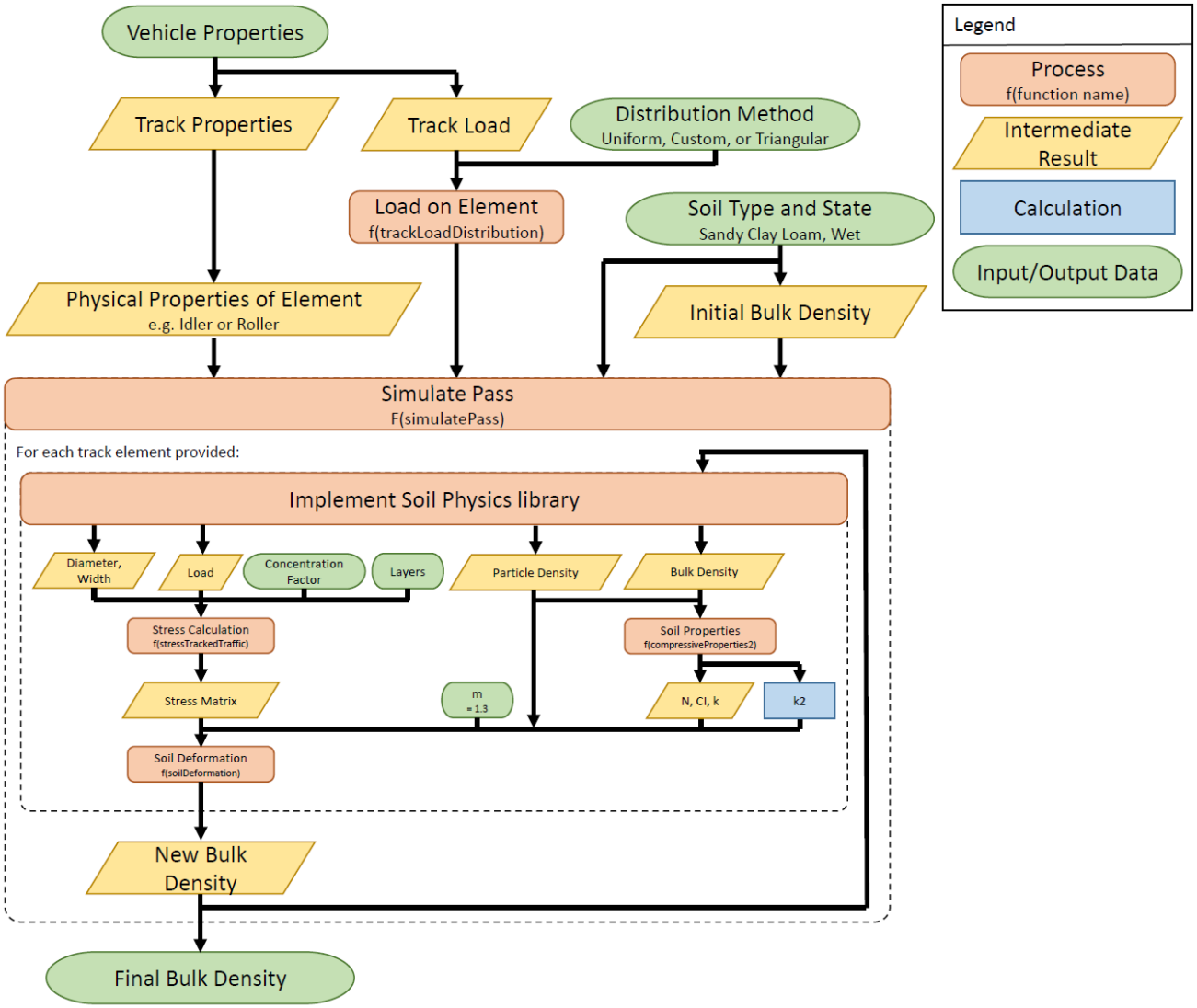

Figure 15: Flowchart of the implementation of the functions and steps involved in the simulating the passing of a vehicle over the soil by using the simulatePass function which provides the final bulk density after all or a selection of elements (wheels, track elements or a full track) has passed the soil.

3.6 Spatial Soil-Track Interaction

Spatial soil-track interaction cover the subject of where the track has interacted with the soil. Based on the guidance path and the physical dimensions of the robot the area affected by the tracks is determined. The methodology is explained in section 3.6.2. First, a description of the path used as input and the generation of this path is provided.

3.6.1 Guidance Path

The path followed by the robot in the field is described by a .txt or .CSV file in which each line corresponds with a point in space which defines a location in terms of an *x*, *y*, and *z* coordinate system. The paths used in this project are generated using the F2C library in a github codespace environment. Additionally, information is given about the direction the robot is facing, the forward speed, the driving direction and if the point belongs to a turning operation or a straight swath (Table 7).

Table 7: Overview of the values presented in the .txt or .CSV file returned by the F2C library.

Property	*Explanation*	*Unit*
Position	x	[m]
	y	[m]
	z	[m]
Angle	Direction related to the x-y plane where an angle of 0 corresponds with the x-axis.	[radians]
Velocity	Forward speed	[m s^{-1}]
Duration	Step size in terms of time	[s]
Direction	1 = Forward, -1 = Backward	
Type	1 = Swath, 2 = Turn	

For this project, the area of interest is the headland of the field. Figure 16 provides an example of the paths for the turns executed on headlands (black lines) stored in the .txt file. These turns are based on a generated result of the F2C library route planning with an arbitrarily shaped convex field. In this project individual turns were the main focus. However, analysis on field scale was also done (section 3.9).

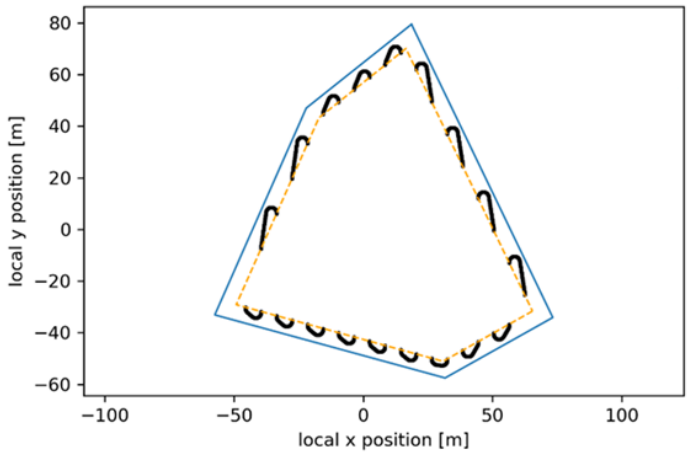

Figure 16: Visualization of the turns for a convex field. The blue line indicates the field border, the orange dashed line indicates the headland border, and the black lines are the guidance paths. The shown curves are Dubins with continuous curvature. The order of the curves is boustrophedon. The field was randomly generated and has an area of 1 hectare.

3.6.2 Determination of the Disturbed Area

As a starting point, the path of the robot is generated using the F2C library. For analysing specific properties of curves, curve sections, and single or multiple turns (Figure 16) were generated. Based on the generated path, new paths are derived using the physical dimensions of the robot (Figure 17). This results in the paths that each ITE has followed during the execution of a turn. The need for this operation comes forth out of the analysis by Li et al. (2007) who indicated that a full track system does not follow a perfect path. This is the result of the physical length of the track where the most front and most rear parts will start skidding related to the COR. The process described here is summarized in the flowchart (Figure 18). The following paragraphs will explain each step of the process in more detail.

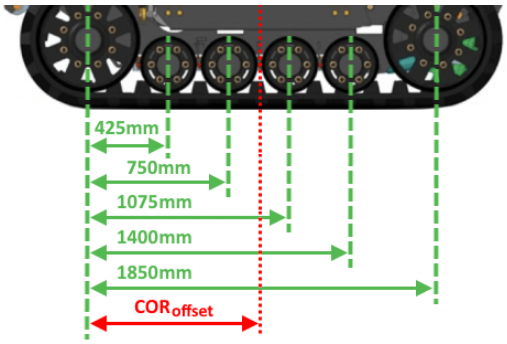

Figure 17: Side view of the AgBot 5.115T2. The values represent the distances between the elements relative to the most front idler [mm]. The values are retrieved from (Appendix B). COR_{offset} represents the distance of the front idler to the centre of rotation of the robot (in this case set to the centre of the track). Retrieved and modified from: (AgXeed, n.d.-a)

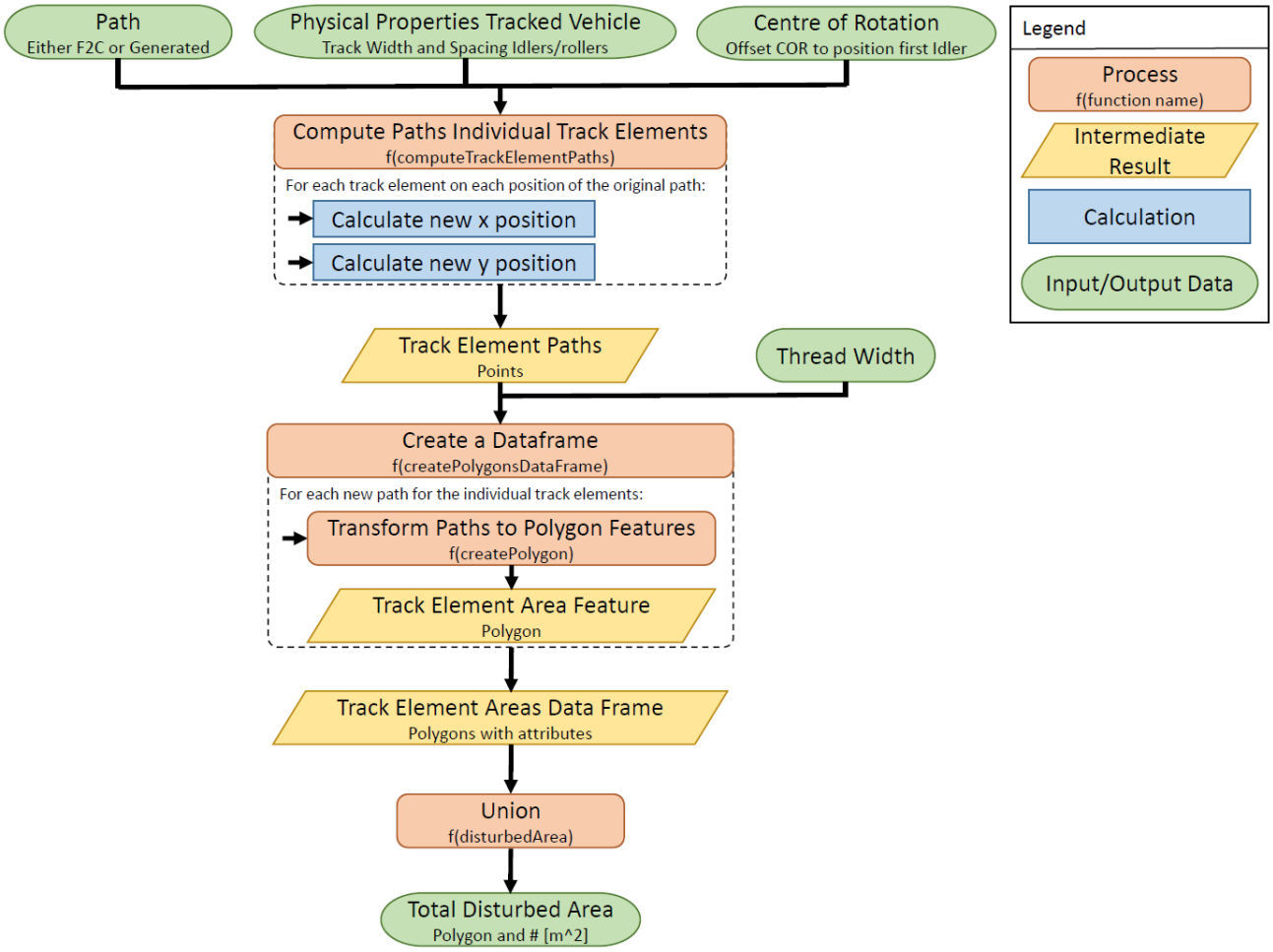

Figure 18: Flow chart of the steps involved and explained in section 3.6.2. At the top the input requirements are given which are used to compute the paths of the ITEs. These new paths are used in a buffer operation with the track width. The generated features are combined using a union operation resulting in a feature of the total DA.

3.6.2.1 Individual Track Element Positions

For obtaining the *x* and *y* coordinates of the ITEs relative to the original path equations 16 and 17 are used. Figure 19 A&B shows the spatial setup supporting the equations. A more elaborated version of this derivation is provided in Appendix E.

$$x_{ITE} = x - cos(\alpha) * \left(\frac{1}{2}TW - tan(\alpha) * COR_{offset}\right) \quad (16)$$

$$y_{ITE} = y + cos(\alpha) * \left(COR_{offset} + tan(\alpha) * \frac{1}{2}TW\right) \quad (17)$$

Where the equations make use of the following variables: the angle (α $[radians]$) as defined in the F2C output (Table 7), the position of the robot (x- and y- coordinates), the COR_{offset} (Figure 17) and the track width (TW, Table 1).

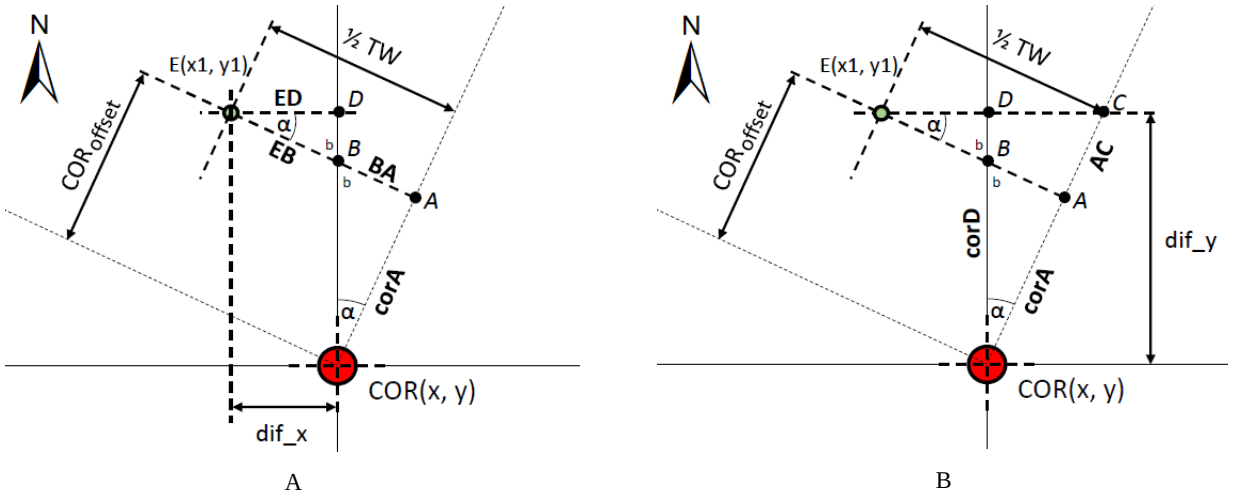

Figure 19: A – Spatial representation of the components used to calculate the new x- coordinate (x1) of the position of one of the individual track elements (E). B – Spatial representation of the components used to calculate the new y- coordinate (y1) of the position of one of the individual track elements (E). For both figures, α, x, y, COR_{offset} and TW are known variables.

3.6.2.2 Disturbed Area Calculation

Applying the methodology for obtaining the position of the ITE relative to the location of the robot along the original path defines a new path for this specific ITE. This process was repeated for each ITE of both tracks. Hereby a total of twelve paths matching each ITE were generated. This process was performed using a python function (*computeTrackElementPaths*). The next step is to make a line object which allows for deriving the area. To do this the shapely library (Shapely, n.d.) was used. This library provides classes and methods for spatial analysis and manipulation of data (planar features). The operation applied in this step is related to transforming the individual points to a line object (till now the path was represented as points). This line object is then buffered. The scale of the buffer is determined by implementing the physical width of the tread of the track (Table 1).

The results in terms of the areas disturbed by the individual track elements are the first quantification of the interaction between the soil and a track system. At this stage, the result contains individual polygons each representing the area covered by one ITE. By performing a union operation (ESRI, n.d.) on these polygons the individual areas were combined to create a (multi-) poligon of the total disturbed area. Using the *.area* operator of the Shapely library the total disturbed area of the single turn (A_{turn} $[m^2]$) represented by a single value was found. These steps were performed using the *spatialPathTrackOperations.py* script (8).

3.7 Combining Bulk Density Change with Spatial Data

For the implementation of the soil compaction aspect concerning the spatial data, the specific area features of the ITEs are required. The goal is to map the compaction based on the track elements which have driven over a specific area. The areas overlapping each other were determined by using Boolean operations (intersection). To do this for all polygon features created for a single track the *cascadedIntersection.py* script was written which handles the splitting of the overlapping polygon features. For these new features, there is a method for checking which elements drive over this specific area. This could be one track element or multiple track elements. This information is provided to the *soilpass.py* script (section 3.3) to calculate the change in bulk density for this specific area. This process is executed for each individual shape resulting from the cascaded intersecting. This generates a spatial pattern including information on the final bulk density in each individual part of the pattern.

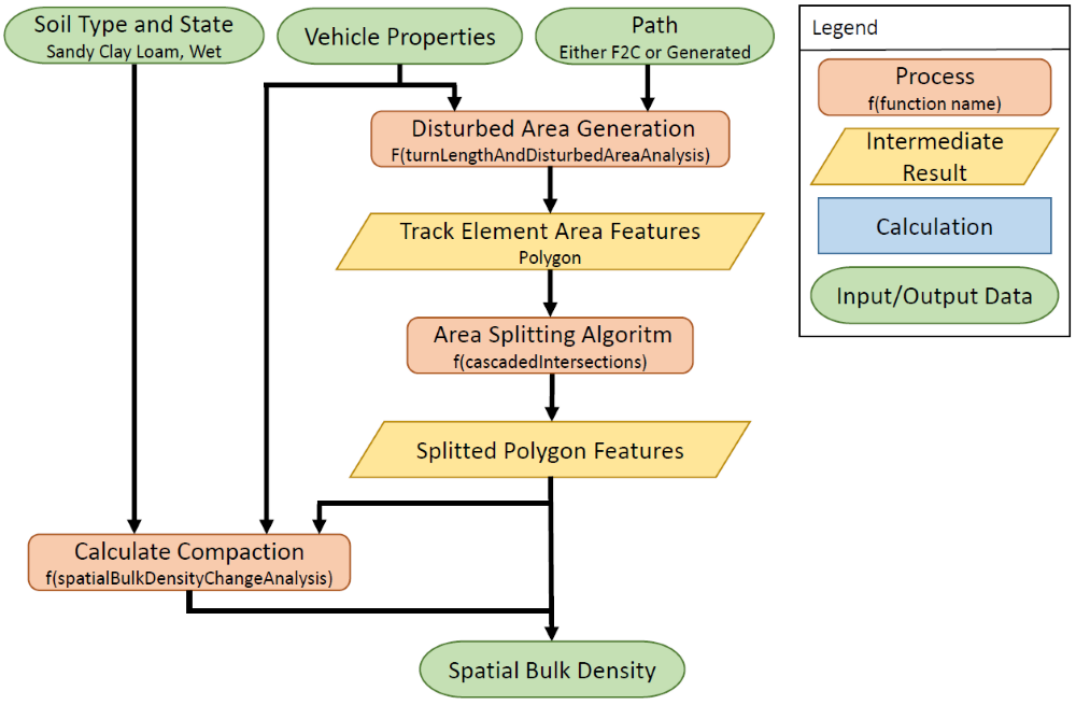

Figure 20: Flowchart describing the steps performed in section 3.7 for generating spatial features based on overlap and linking the fBD to these specific areas.

3.8 Sensitivity Analysis

By performing a Sensitivity Analysis (SA) the influence of the different input variables representing for example the different configurations of the robot, the soil state, and the specific turn types were investigated. In the case of this project, a one-at-a-time (OAT) SA was performed. An OAT SA means that only a single variable/parameter is changed, and all others remain the same. This requires the definition of a reference situation to which all changes were compared. For both, the change in BD and DA, a SA was performed. The reference situation is defined below and Table 8 gives an overview of the changes in parameters which are applied in the AOT SA.

For the BD SA, the OS and TS were considered separately, and the reference situation was defined as follows: the tread width is 0.610m; the pressure distribution is uniform for the OS and custom for the TS; the soil state is wet; the de Lima calculation method is used; the soil type is Sandy Clay Loam; and the iBD is 1.37 $Mg\ m^{-3}$.

For the DA SA the standard situation was defined as: the tread width is 0.610m; the track width is 2.250m; the turn type is Dubins with continuous curvature; The turn radius is 2 m; the x offset, related

to the working width, is 3 m; the y offset, related to the headland angle associated to the working direction, is 0 m; and the heading, which is related to the shape of the turn and the angle between the headland and the working direction, is 0 degrees which denotes a north-south orientation.

Table 8: Overview of the parameters changed in the AOT SA, and which values or settings of the parameters where used.

Subject	*Parameter*	*State*
Robot	Track Configuration (tread width / track width)	300/1800, 300/3200, 610/2250, 610/2850, 910/2350, 910/2850
	State	Operating, Turning
	Pressure Distribution	Uniform, custom, or triangular
Soil	State	Wet or dry
	Method	O'Sullivan or de Lima
	Soil type	Sandy loam, sandy clay loam
	Initial Bulk Density	1.37, 1.3837, 1.3974, 1.4111, 1.4248 (5% increase)
Turn	Type	Dubins, Dubins with continuous curvature, Reeds-Shepp, or Reeds-Shepp with continuous curvature
	Turning radius	2, 3, 4, 5 m
	Swath width	3-12 m in steps of 0.5m
	Angle	0, 15, 30, 45, 60, 75, 90 degrees
	Y-offset (relates to the angle of the headland compared to the angle of the working direction)	0-12 m in steps of 0.5m

For the comparison a sensitivity plot was made. In the (to be) created plot the input variables and the output values were normalized. For the quantitative variables an ordinal scale is used to distinguish their position on the x-axis. The normalization is specified in equation 18.

$$s_n = \frac{s_{in,out} - s_s}{s_s} \quad (18)$$

Where, s_n is the normalised state value related to the input or the output of the model. $s_{in,out}$ is the input variable for the model or the output value resulting from running the model. s_s represents the value for the selected standard situation.

For example, applying equation 18 to the tread width of 0.300m with the standard of 0.610m as an input state yields the following normalization:

$$s_{n,tread\_width} = \frac{0.300 - 0.610}{0.610} = -0.508$$

3.8.1 Defining Objective Functions

The F2C library currently makes use of a brute-force optimizer. This optimizer handles the provided objective function and calculates solutions by employing an exhaustive search over a discretized solution space given the minimalization or maximalization problem related to the objective. The selected solution for the CPP problem is selected based on optimal solution. Introducing the new quantifications described in this report, new cost functions were defined. The goal is to provide a selection of new cost functions related to the new quantifications as a recommendation for expanding the F2C software capabilities.

3.9 Field Scale Analysis

The performed sensitivity analysis provides insight into which parameters have the largest influence on the results and how they influence the result. This knowledge was put to the test by comparing the results on a field scale. This was done solely for the DA analysis. The analysis of compaction related to the spatial situation described in section 3.7 is too computationally intensive.

In the analysis of the whole field using the generated path the currently implemented optimizers were tested. This included a selection of a custom angle, the optimization for the total length and the optimization for the number of swaths. Additionally, the turning patterns were compared. The available patterns are boustrophedon, here the swaths are cultivated in consecutive order. Furthermore, there is the snake pattern, here one swath is skipped and filled in when the other side of the field is reached. Lastly, there is the spiral pattern. For this pattern, the field is cultivated in blocks from which the number of swaths of each block is defined.

3.9.1 Convex Field

For the analysis on field scale, a field was generated using the F2C library. The code to do this is provided in Appendix F. For this project, seed 42 was used for creating a random field of 1 ha with 5 sides (Figure 21). The headland width has a fixed width of 12 m which is indicated by the dashed orange lines in Figure 21. The coordinate system used is a local planar coordinate system.

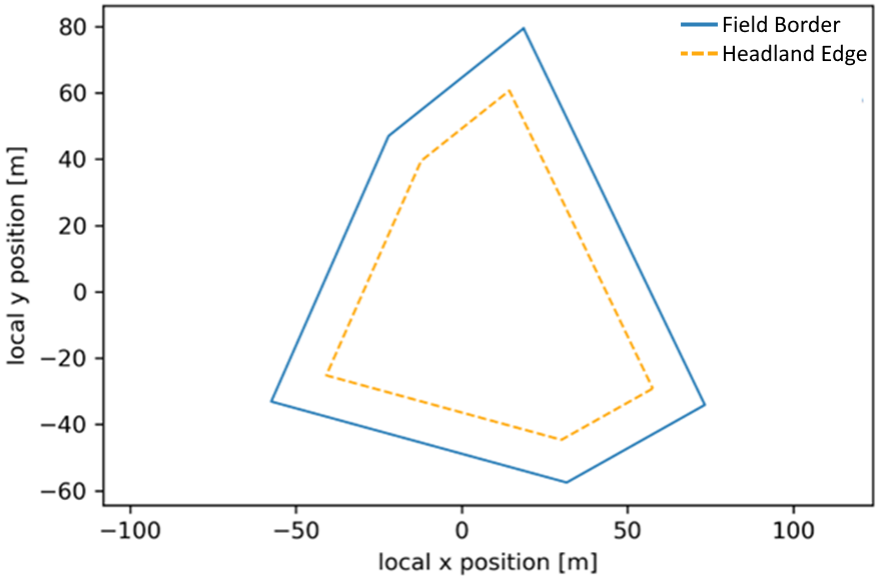

Figure 21: Artificially generated convex field with an area of 1 hectare and 5 sides. A local coordinate system is applied represented in metres. The field border is indicated in blue and in yellow the headland edge is indicated. The distance between these lines is 12 m in this case.

4 Results

4.1 Soil Model

The stress matrices contain information on the pressure pattern applied by the ITE on the area below the ITE. For a single idler and roller, the patterns were visualized based on a top-down view in Figure 22 A&B. The values in the figure represent the stress [kPa] related to the regions identified with the contours. The patterns are cut off in terms of the contact width, this is caused by model limitations. This means that only data is available for the set physical contact with of the track, which is 0.510m in this example. It is observed that the pattern below an idler has a significantly smaller footprint in terms of the contact length. This has resulted in higher peak stress at the center of the contact area which was explained by equation 6 introduced in section 2.2.1. The stress patterns provided are based on a track with a tread width of 0.610 m and a load of 650 kg on each ITE (implying a uniform distribution of the load on the track). The soil-related properties which are represented by the soil layers and the concentration factors were set as described in section 3.2.

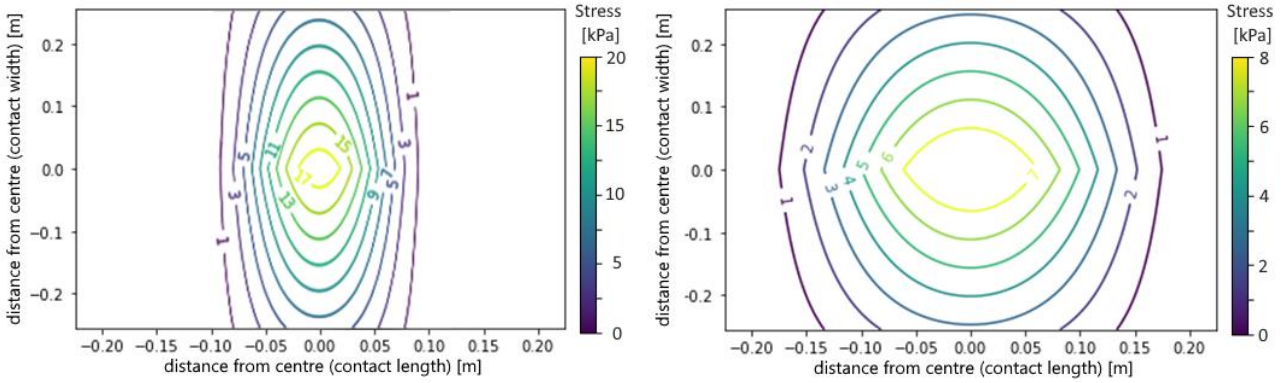

Figure 22: Stress patterns for an idler (A) and a roller (B) of the track of the AgBot based on a uniform distribution leading to a total load of 650kg on each track element. The width of the track is set to be 610mm which means a width of 510mm is used on the model (Keller & Arvidsson, 2016). The values in the figures represent the stress in kPa.

The pattern stored in the stress matrix can also be visualized in 3 dimensions. This makes a stress profile (Figure 23). Based on the shape of this profile the modifications in the *stressTrackedTraffic* module was validated by comparing the front and side view with the patterns in the original paper by Keller and Arvidsson (2016). It is found that the overall shape of this stress profile corresponds with what is expected considering the paper.

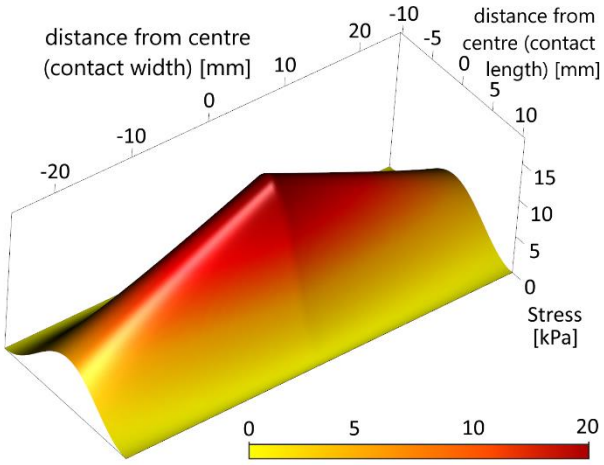

Figure 23: Stress profile of the front idler with a load of 650 kg.

This stress pattern is used as an input for the *soilDeformation* module and here it was found that applying a load of 650 kg on the front idler results in an fBD of 1.3991 [$Mg\ m^{-3}$]. This means the BD has changed with 0.0291 [$Mg\ m^{-3}$] ($= fBD - iBD = 1.3991 - 1.37$). So, the observed compaction is 0.0291 [$Mg\ m^{-3}$].

4.2 Soil-Track Interactions

4.2.1 Compaction

The soil track interactions treated in this project are the compaction and the disturbed area. Compaction is defined as the change in BD. The previous paragraph provided the result, in terms of compaction, by processing a single roller or idler. Section 3.5 explains how this method is expanded and applied for a full track by looping over the ITEs. Additionally, the two states of the robot related to the pressure distribution of the track were introduced. Applying this methodology has led to the generation of results as was observed in Figure 24.

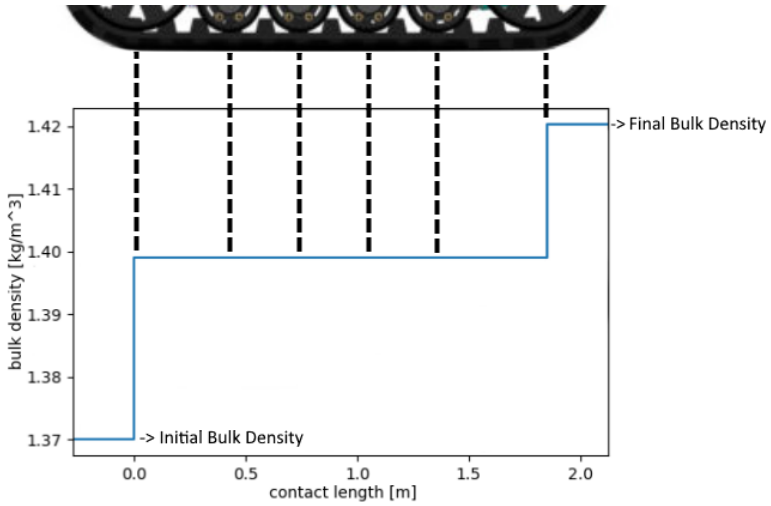

Figure 24: Quantification of the change in bulk density after the passing of consecutive elements resulting in a change of bulk density from $1.37\ Mg\ m^{-3}$ *to* $1.4204\ Mg\ m^{-3}$*. The weight applied is that of the robot with a uniform distribution and the state and soil type used is wet Sandy Clay Loam.*

In this example above the load distribution on the track is uniform and the total load is based solely on the weight of the robot. For this project two states, OS and TS, of the robot were considered. For both of these variations, Figure 25 A&B provides the results. It is observed that both, the distribution, and the total load play role in the observed changes. The increased load makes that the fBD is larger and th alternative load distributions results in a different step pattern.

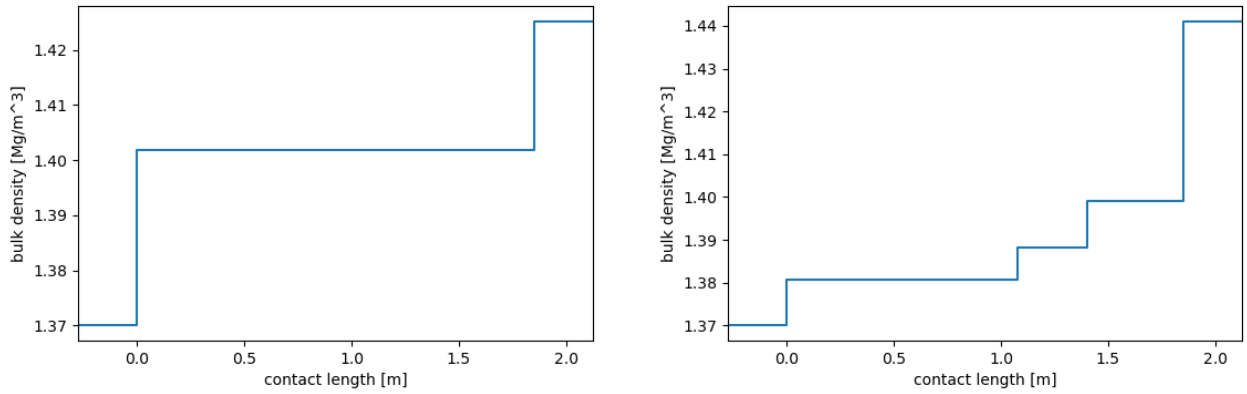

A B

Figure 25: Compaction patterns by a pass ofof the AgBot. A – Operating state of the AgBot with a uniform load distribution. The change in BD is $0.0552\ [Mg\ m^{-3}]$ $(= 1.4252 - 1.37)$*. B – Turning state of the AgBot with a custom load distribution leading to a compaction value of* $0.0711[Mg\ m^{-3}]$ $(= 1.4411 - 1.37)$*. The soil in both models is wet Sandy Clay Loam as described by de Lima et al. (2018)*

In the operating state (Figure 25A), where the load of the robot and implements is uniformly distributed, it is observed that the idlers cause compaction. This was explained by the difference in the stress patterns as was observed in Figure 22. The rollers have no direct influence on the measured variable in this case. Comparing the resulting BD of this image with the one of the Agbot without the implements (Figure 24) shows that a higher load leads to an increase in the fBD implying more compaction.

The pattern observed in Figure 25B has a significantly different shape which was traced back to the load distribution on the track. Furthermore, the fBD is higher which was expected as a higher load is applied and the stress on the soil is more localized on a few of the ITEs at the rear of the track.

4.2.2 Disturbed Area

An overview of the disturbed area results, concerning a single turn, ---as a proof of concept---, is given in Figure 26 and Figure 27. First, the points of the original path were used to calculate the position of the ITEs providing the path of an ITE (Figure 26A). This process was repeated for each ITE. This way 12 new paths were obtained (Figure 26B). The figure with all paths shows the skidding behaviour of the track. This can especially be observed at the inner track where the deviations between the paths of the ITEs are noticeable.

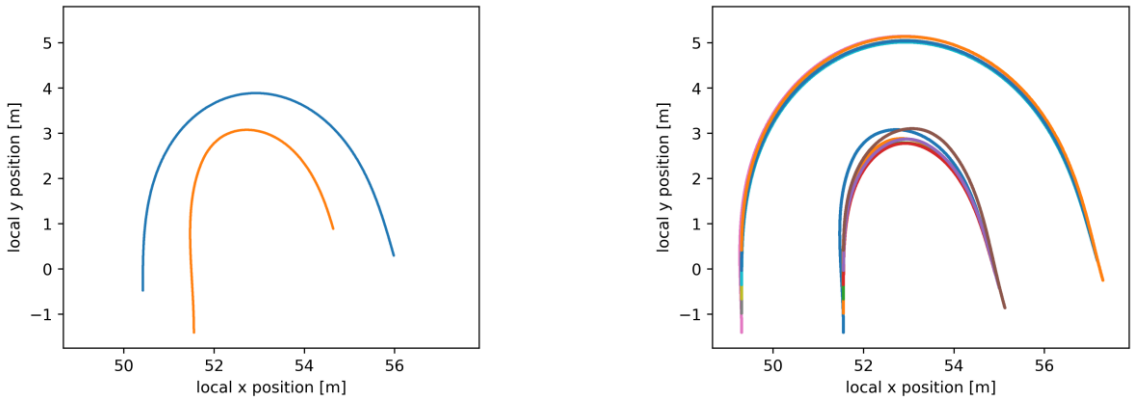

Figure 26: Processing of the original path (the blue line in A). The COR_{offset} was set to the physical centre of the track of the robot (0.925m) A – The blue line represents the original path used for the guidance of the vehicle. The orange line indicates the path the front left idler follows during the turn. B – There are a total of twelve paths, each representing an individual idler of roller of the left or right track.

The final product is obtained after applying the buffer operation which results in the areas corresponding to each ITE (Figure 27). These individual features are combined into two features, one for each track using a union operator. These resulting areas described by polygon features indicate the total disturbed area. From the feature, a numeric value was derived which gives the total disturbed area of features.

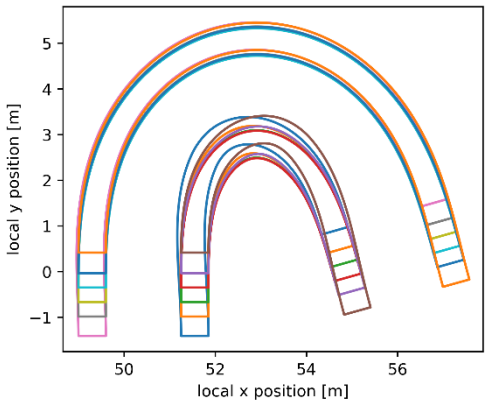

Figure 27: Soil contact areas of the ITEs. In this case a tread width of 0.610m was used.

The application on an individual turn scale will be represented using the test field with a generated solution of the F2C library. This has resulted in a total of 18 turns required for manoeuvring the robot to a new swath to cultivate the whole field. It was observed there are duplicates of the same curve configuration. Therefore, the unique curves are detected (Figure 28) using the *uniqueTurnDetection.py* script (8) created to be used in the F2C codespace environment.

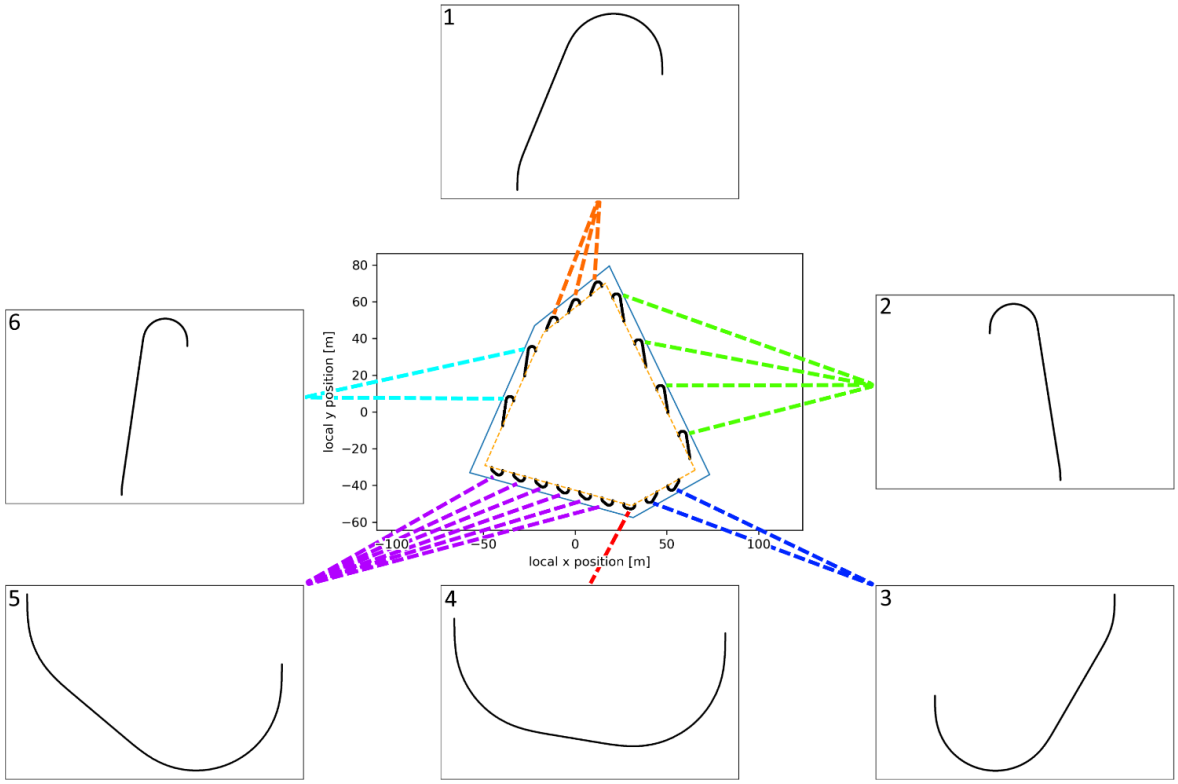

Figure 28: Unique curve configurations for the artificial 1 ha field. The ww of the implement was set to 6 m, the turn type is Dubins with continuous curvature with a set radius of 2 m. A total of 6 unique curve configurations were identified.

Accordingly, the DA is quantified for each unique turn. For a selection of turns the result were observed in Figure 29 A&B. The additional results are to be found in Appendix H. For turns number 1&2 the DA is 26.44 m^2 and 35.56 m^2 respectively. The skidding of the tracks was observed in both figures. Especially at the inner track (blue). This observation corresponds with what is expected based on the theory of the disturbed width.

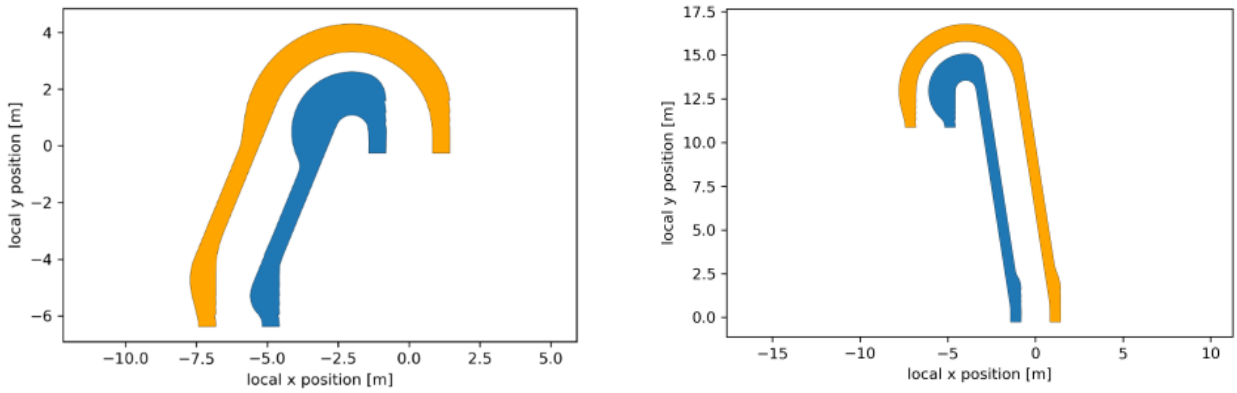

A B

Figure 29: Footprint of the disturbed area based on the standard configuration of the AgBot. A - The result of turn 1 from Figure 28. B - The result of turn 2 from Figure 28. The orange corresponds with the right track and the blue corresponds with the left track of the AgBot.

4.3 Sensitivity Analysis

The sensitivity analysis provides a graphical way of identifying patterns related to the input variables. The patterns show which variables have the greatest influence on the model. This indicates what variables need to considered at specifically in terms of applying the models.

The SA was split in terms of compaction (fBD) and DA. The data and values related to this SA can be found in Appendix H. First, the results and findings related to compaction are discussed. The graph below shows the data points of the normalized BD values related to the normalized input variables (Figure 30). The graph corresponds to the analysis of the TS as this was the focus of the project. However, in Appendix I the result of the OS is also added.

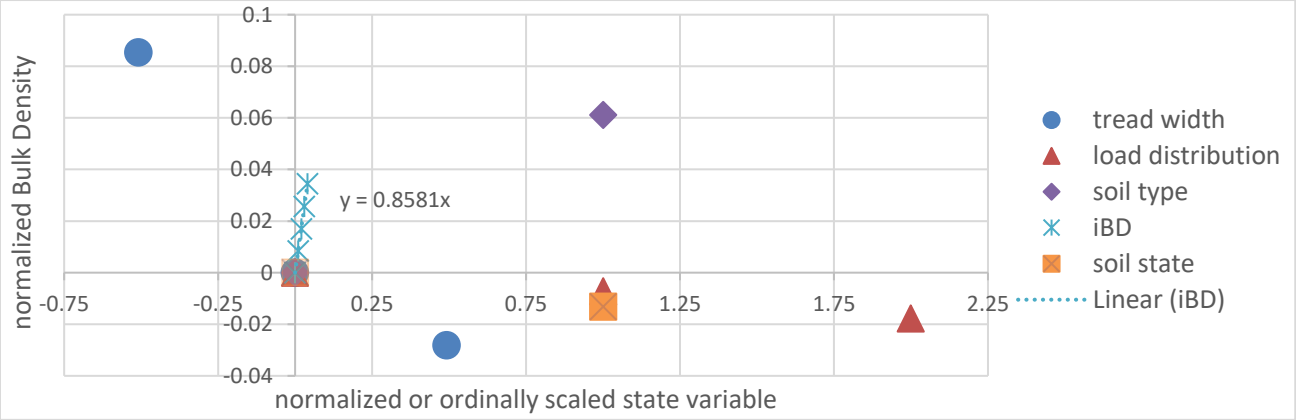

Figure 30: Sensitivity analysis of the bulk density on the AgBot in the turning state. The Tread Width and iBD are quantitative variables and the others are qualitative variables. Load distribution: 0 – Custom, 1 – Uniform, 2 – Triangular. Soil type: 0 – Sandy Clay Loam, 1- Sandy Loam. Soil state: 0 – Wet, 1 – Dry.

Tread Width: The trend indicated by the data points shows that a wider track causes less compaction. This effect is especially present during the turning operation as the total load on the track is higher compared to the OS. Having a track half, the size of the standard situation (so, 300 mm instead of 610 mm) makes that the BD increases by 8.5%, and having the track with a width of 910 mm results in a decrease of 2.8% compared to the standard situation.

Load Distribution: The load distribution is a qualitative variable. There were 3 options available (uniform, custom, and triangular). The custom distribution (0) described for this project results in the highest fBD. Followed by the uniform distribution (1) and then the triangular distribution (2) shows to resulting in the lowest compaction during a turn. This is rather unexpected as this pattern was thought to represent the turning state.

Soil Type: Based on the results for both soil types, it is found that sandy soils are more prone to compaction. For the same situation on the different soil types, a 6.1% higher fBD is observed on clay soils. This effect was substantiated by the fact that clay soils are less porous and thus are less susceptible to compression.

iBD: An increase in the iBD results in an increase in the fBD. The relation was described by a linear formula (Linear (iBD) in Figure 30). This indicates that when the iBD increases by 1% the fBD increases by 0.86%. This relation was not expected regarding literature. Compacted soils were harder to compress implying a declining effect of the iBD on the fBD which is not observed in the results.

Soil State: Dry soils have been found, considering the SA, to be less susceptible to compaction.

In the methods was described that the two calculation methods by O'Sullivan and De Lima would be compared. However, using the methods by O'Sullivan no change in the BD was observed making the results inconclusive (Appendix H).

For the disturbed area, the number of variables tested was greater and this led to the graph shown in Figure 31. It was observed that the original graph contained data points that indicated some unexpected behaviour. Therefore, these have been removed from the graph below. The full graph is to be found in Appendix J. The graph shows the SA for the DA. For a selection of the quantitative variables, the trendlines were added to gain insight into the relationship between the input values and the resulting output. The findings and observations related to the contents of the graph are discussed below the graph. The graph solely contains the SA data on the DA. However, in the analysis, the results of the turn length and overlap introduced by the turning operation are also covered below the graph.

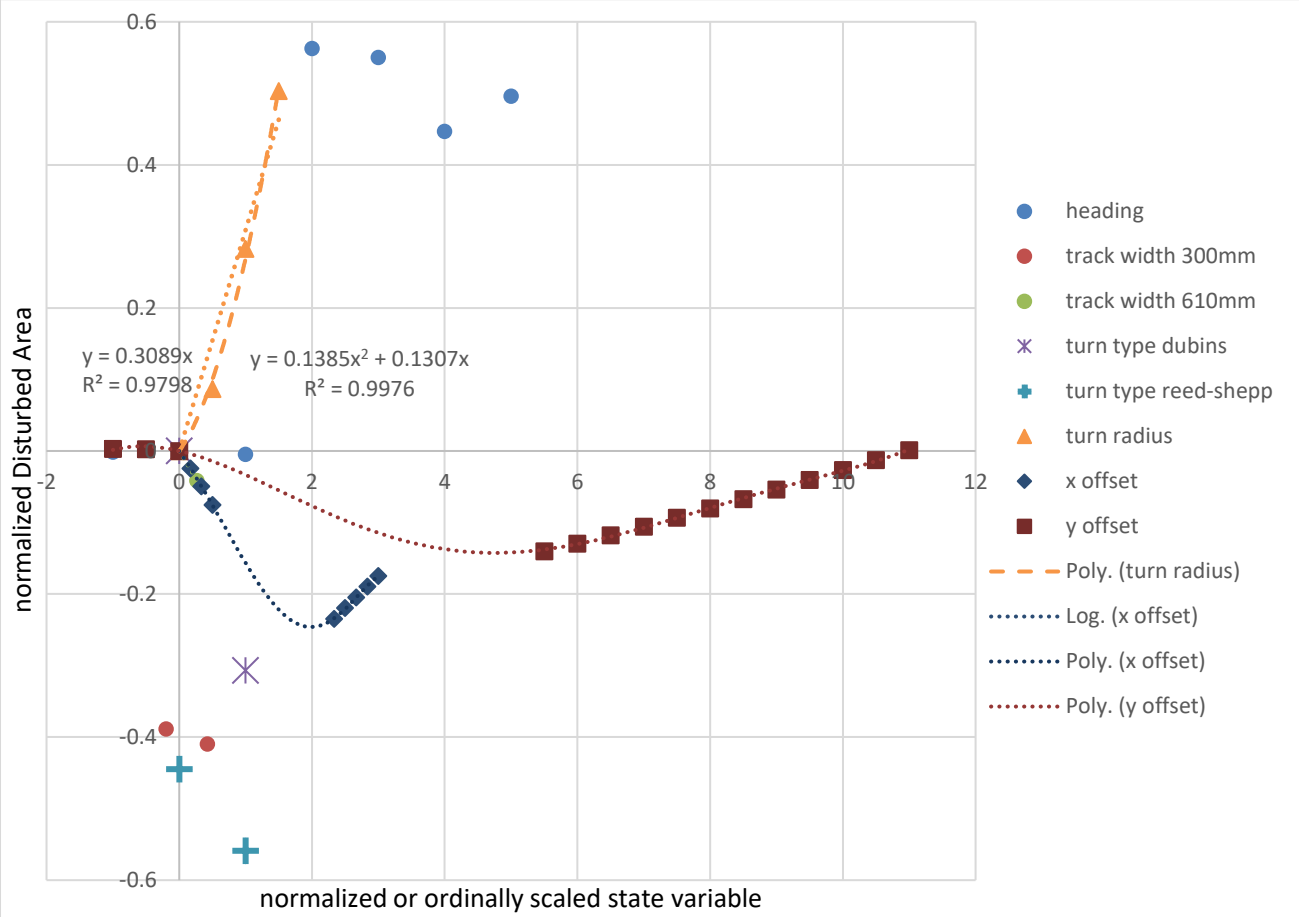

Figure 31: Sensitivity analysis on the Disturbed Area on the described input variables using the variables stated in Table 8 as the reference state. For the turn types, both Dubins and Reeds-Shepp are presented with continuous curvature (0) or in their normal form (1).

Heading: The results of the heading indicated there is a threshold related to the angle for which the DA increases significantly. When the selected angle was greater than 30 degrees the DA increased significantly. For angles smaller than 30 degrees a decrease of maximal 0.4% related to the set standard angle of 15 degrees was found. In terms of the length of the turn based on the set path, it was observed that having a work direction perpendicular to the headland edge seems to result in the lowest path length. Accordingly, the DA was also found to be the lowest in this situation. The results on overlap show that for angles greater than 45 degrees, the overlap is introduced irrelevant to the turn type. When the angle is 75 or 90 degrees a significant amount of overlap, 5,8% and 3,7% respectively, is introduced. Note that an angle of 90 degrees will probably not be experienced in practice.

Tread Width: The relation found for the tread width is that with a wider tread of the track the disturbed area becomes larger (Figure 32). This is expected as the width is integrated over the length of the track. This also shows that the skidding effect, which is found to be more significant for narrower treads (300mm), does not outweigh the effect related to the physical size of the track (Figure 32).

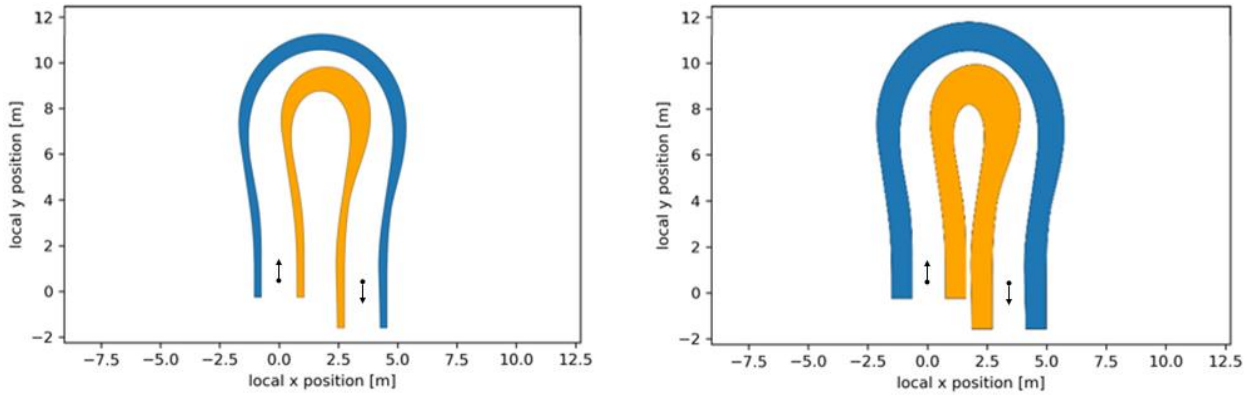

A B

Figure 32: Disturbed areas using two different track configurations in terms of the tread width. In both plots, the same path is used to generate the resulting DA. The x-offset is set to 3.5 m and the y-offset is 0 m with a heading of 0 degrees. The arrows indicate the driving direction. A – Resulting DA pattern for a track configuration with 300mm wide treads, the total DA is 24.09 m^2. B – DA pattern with 900mm wide treads resulting in a total DA of 54.48 m^2.

Track Width: Comparing the track widths for different tracks with different tread widths it is found that the robot with a wider track stance has disturbed less area compared to the standard narrow track. A decrease of 4.2% was realized (610mm tread) using the same tracks with a wider stance. This implies that, related to the ww of the implements, having a wider track width is preferred when the DA is to be minimized.

Turn Type: For the turn types it was observed that the Reeds-Shepp variation always provided a shorter turn compared to the Dubins turn variant. This relation is also found for the DA. One aspect of the Reeds-Shepp variation is that this type of turn introduces overlap (Figure 33B). This is one of the benefits of this turn type which makes that this variation overall leads to a lower DA. The continuous curvature variations used for both turns showed that this type always resulted in a larger DA as less instantaneous turning is allowed for these variations.

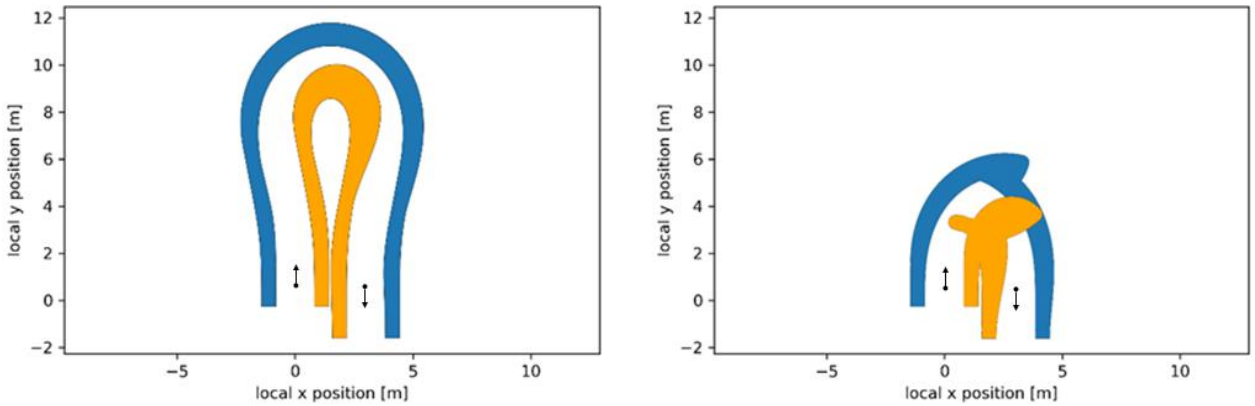

A B

Figure 33: Disturbed areas using two different turn operations. In both plots the same start and end position was defined. The x-offset is set to 3 m and the y-offset is 0 m with a heading of 0 degrees. The arrows indicate the driving direction. A – Resulting DA pattern with the continuous curvature Dubins variation, the total DA is 40.55 m^2. B – DA pattern with the continuous curvature Reeds-Shepp variation resulting in a total DA of 22.52 m^2.

Turning Radius: Increasing the minimum turning radius results in an increase in the length of the path required for the turn and the DA of the turn (Figure 34). This result is expected. However, an interesting aspect of this is that the behaviour of increasing the minimum turning radius is not linear with the increase in the disturbed area (Figure 31). Considering the R-square fit (visible in Figure 31) to the datapoints of the turning radius, it was found that using a polynomial fit gives a better representation of this relationship. Knowing this relation makes it possible to estimate the effect using a different turn radius based on the generation of only one single result.

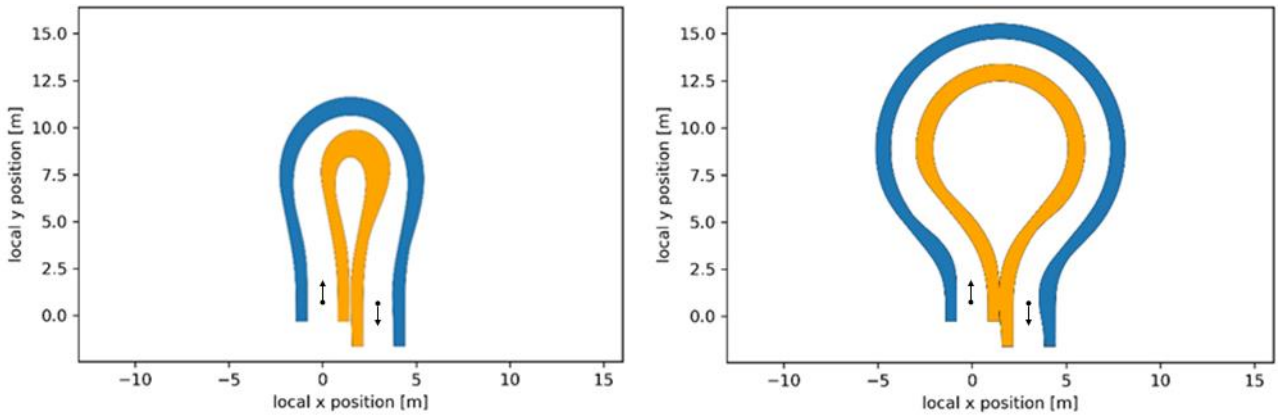

Figure 34: In both plots, the same path is used to generate the resulting DA. The x-offset is set to 3 m and the y-offset is 0 m with a heading of 0 degrees. The arrows indicate the driving direction. A – Resulting DA pattern with the continuous curvature Dubins' variation with a minimum turning radius set to 2 m, the total DA is 40.55 m^2. B – DA pattern with the minimum turning radius set to 5 m resulting in a total DA of 60.97 m^2.

x-offset: The first step in considering the results for this aspect was filtering them based on the realism of the application in practice. For a selection of the results, the generated paths were unrealistic as they involved circular turning operations. For the resting data points, it was found that by increasing the *x*-offset (the lateral offset), which is related to the implement width, the DA will first decrease and after some threshold is passed the DA starts to increase again. This indicates there might be an optimal working width related to the configuration of the AgBot in correspondence with the turn radius.

y-offset: For the analysis of the y-offset, an offset of 1 m is set as a reference. In this case, a similar problem is found in the previous paragraph. Certain values for the *y*-offset resulted in the generation of unrealistic turns. Again, these data points are removed from the graph. Looking at the results it was observed that by increasing the y-offset (longitudinal offset) initially the DA decreased and for larger values for the *y*-offset the DA increased again (Figure 31).

4.4 Convex Field

The working width of the robot is set to be 3 m and the turning radius is also set to 3 m and the instantaneous curvature change for the continuous curvature variation is set to 0.25. In this paragraph, the results are represented in a specific order. The starting situation is the implementation of Dubins curves with continuous curvature and the swath ordering method is boustrophedon. This situation will be compared to the situation with an optimized swath pattern for the inner field and the alternative ordering types will be tested.

For selected situations, the results are presented in Table 9 which provides the quantitative data. The corresponding figures can be found below the table or are provided in Appendix K. The observations in the data and an analysis of the figures of the resulting DA patterns are discussed.

Table 9: Full field analysis with the listing of the used settings and the resulting DA in terms of square metres and as a percentage of the whole field.

#	Swath Pattern	Direction	Turn Type[1]	# Turns	DA [m²]	DA [%]	Image
1	Boustrophedon	Custom Parallel to y-Axis	Dubins	32	3397.12	34.0	Figure 36
2	Boustrophedon	Custom Longest Field Edge	Dubins	28	3254.82	32.5	Figure 36
3	Boustrophedon	Optimized for Length	Dubins	31	3355.62	33.6	Figure 36
4	Boustrophedon	Optimized for Number of Swaths	Dubins	28	3305.03	33.1	Figure 36
5	Boustrophedon	Optimized for Length	Reeds-Shepp	31	2725.61	27.3	Appx. K
6	Snake	Optimized for Length	Dubins	31	3046.90	30.5	Figure 37
7	Snake	Optimized for Number of Swaths	Dubins	28	3110.26	31.1	Appx. K
8	Spiral (n=4)	Optimized for Length	Dubins	31	3188.70	31.9	Figure 37
9	Spiral (n=4)	Optimized for Number of Swaths	Dubins	28	3078.58	30.8	Appx. K

[1] In this table the selected turn types are always of the continuous curvature variation.

According to the DA values in Table 9, pattern 5 would result in the least disturbed area. This is mainly caused by the Reeds-Shepp turn variation. However, considering the spatial pattern of this result it was observed that the turning operation is not executed on the headland area dedicated to the turning operation (Figure 35). Instead, the robot resulted turning inside the cultivation area, which is to be averted. This indicates that for the analysis of these results, the visualization is of great importance besides the numeric results. The main reason being the identification of the validity of the result.

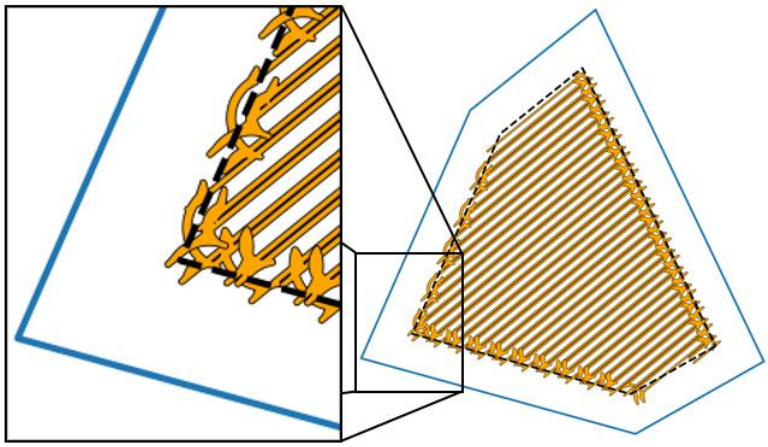

Figure 35: Detail figure of the Reeds-Shepp turning pattern providing insight into the location of where the turning operation is executed.

For patterns 1 to 4 the resulting figures are shown in Figure 36. It was observed that the selection of a specific direction may results in a optimal situation in terms of the DA. Using the standard configuration of the robot (section 3.3.1), the settings in the first paragraph of this section and implementing a direction parallel to the y-axis have resulted in pattern 1 shown in Figure 36A. For the test field with a total area of 1 hectare (10.000 m^2), the total DA was found to be 3397.12 m^2. This means that about 33.4% of the total area of the field was used to drive on for the cultivation of the area within the headlands. Using an optimization or selecting a direction that makes more sense a decrease in the total DA of 1.5%, 0.4%, and 0.9% respectively was realized. Furthermore, it stood out that considering these four patterns, the situation with the lowest DA did also have a lower count in turns: 28 for Figure 36 B&D (patterns 2 and 4) compared to 31 and 32 turns for Figure 36A (pattern 1) and Figure 36C (pattern 3) respectively.

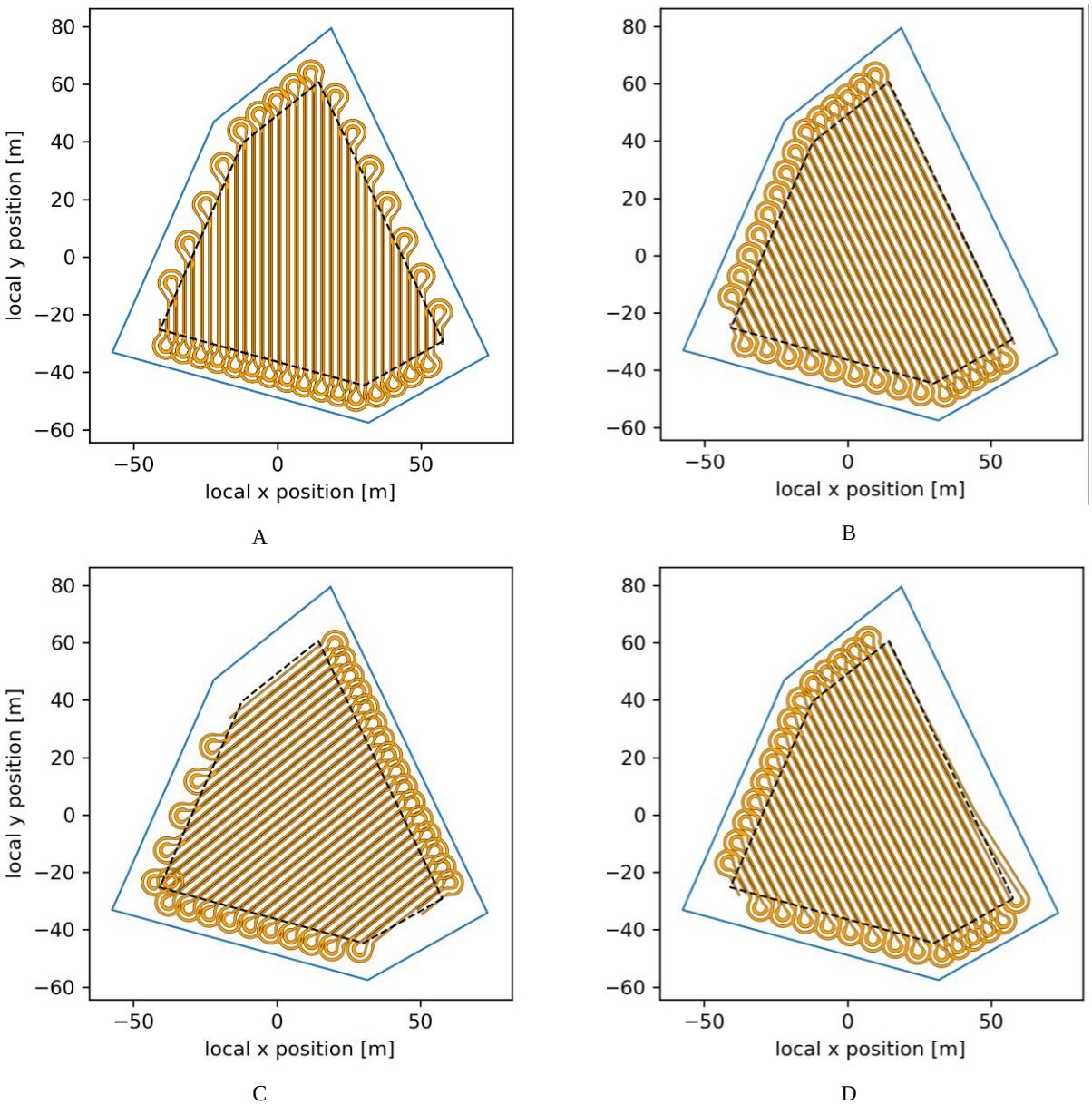

Figure 36: The resulting DA pattern for the convex test field. A boustrophedon pattern is used. A – Pattern 1, using a custom direction parallel to the y-axis. B – Pattern 2, direction perpendicular to the longest field border. C – Pattern 3, with the direction based on the optimization for the total length of the path. This pattern contains one mistake as a circular pattern is introduced based on the generated path (at the sharp corner at the down left part of the figure). D – Pattern 4, with the direction optimized for the number of swaths.

In Figure 37 two alternative solutions for pattern 3 (Figure 36C) are given. Here the swath ordering pattern was changed. Implementing the snake pattern resulted in a total DA of 3046.90 m^2 which is 3.1% less compared to using the boustrophedon pattern. For the spiral pattern, the total DA was 3188.70 m^2. So, this pattern does also have a better performance compared to the boustrophedon swath ordering method. In the figures, the reason for this difference was observed. In both cases, the DA on the headlands shows to be more compact as a result of skipping a swath in most cases. This means less distance was travelled on the headland which has a significant influence on the DA on the headlands. Relating these results to the configuration of the robot and the ww of the implement initiated the thought that an implement of 3 m wide showed to be on the narrow side considering the set turning radius. When swaths are skipped, making the swath-to-swath turning distance 6 m or more, it shows that in some cases a lower impact on the soil is exerted in terms of the DA on a field scale.

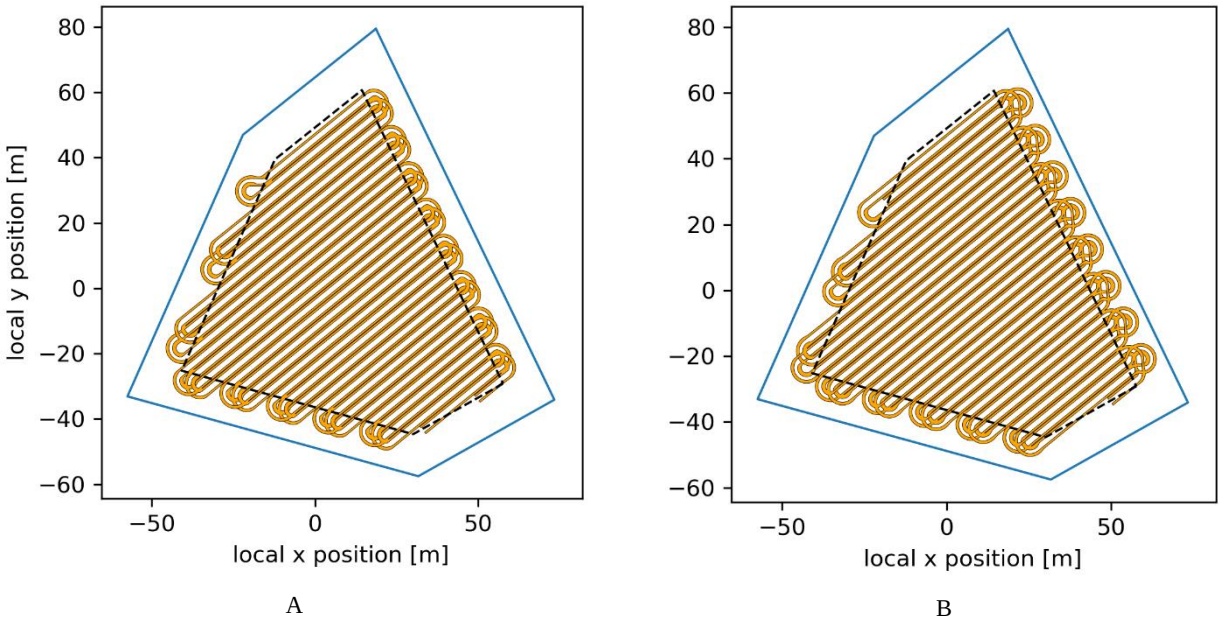

A B

Figure 37: The resulting DA patterns which are optimized for the total length of the swaths. A – Using the snake ordering method. B – Using the spiral ordering method with n=4.

4.4.1.1 In Situ Test

During the project, Gonzalo Mier performed a field test where the robot was set out to follow a generated path pattern. After the robot had driven this path drone images were taken of the field. This made it possible to compare the generated results using the methods suggested in this report with the actual DA caused by the robot. During the execution, it was found that the turning radius of the robot was set to tight which made it hard for the robot to follow the set path. In Figure 38 a section of the field with the results of this test is shown.

It is observed that neither of the methods used for calculating the patterns corresponds perfectly with the situation observed in the field (Figure 38). However, to get a better approximation the DA patterns should be calculated based on the path the robot has actually driven instead of the generated path for the robot to follow. As in practice these paths will not be the same.

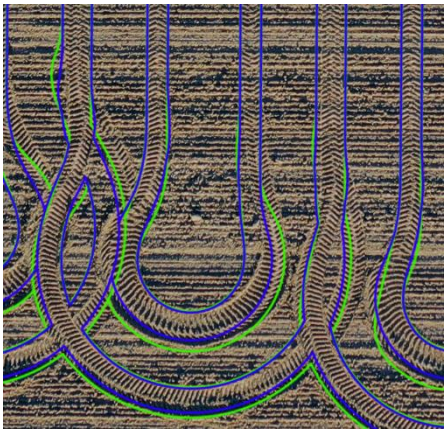

Figure 38: Selection of a drone image of the field where the AgXeed Agbot 5.115T2 drove a predefined path. The image has an overlay of two implementations for calculating the DA. The blue line represents the exterior of the DA generated using the operating state and the green lines represent the turning state.

4.4.2 Objective functions

The new quantification methods and the significance of the variables related to the models provide information that could be implemented in the brute-force optimizer of the F2C library. Below several suggestions of cost functions based on the results of this project are listed as a suggestion for future research and possible expansion of the F2C software. In this project, these suggestions have not been tested or analysed in depth.

Minimizing the total DA. Considering the new quantification method it is of interest to see what this additional information related to the path could add related to the optimization. With the minimization of the DA, the goal is to make the footprint of the vehicle in the field as small as possible. This also implies that overlapping paths will be preferred in the turning operations. The approach for this minimization could be to consider the whole field or only the turns. Which of these options results in the best optimization requires further analysis.

Minimize the compaction by reducing the increase in BD. This is less relevant for optimizing turns however this could be linked to the decision-making to see if the conditions are right for operations in the field. Relating the expected compaction to the current soil state could provide insight into the suitability of the to-be-performed operation. Alternatively, the compaction could be used as a weight for the DA. This could be done by splitting the headland area and non-headland area and multiplying the DA in these areas with the change in BD.

Minimize the distance between the start and end points of a turn. In the results on the field scale, it was found that in some cases the robot has to travel relatively long distances to reach the next swath. Especially, for the first or last few turns when only small paths need to be cultivated. This has risen the thought of considering this driven distance in the optimization. This could be implemented by minimizing the distances between the end and start of consecutive swaths. Also related to the turns, it could be interesting to minimize the number of turns. This is possibly closely related to minimizing the number of swaths. However, there is no analysis being performed to see if this is the case.

4.5 Spatial Compaction

One aspect discussed in the methods has not been explicitly covered in the results. This is the combination of the compaction aspect and the DA. It was found that the *cascadedIntersecting* operation was not very efficient which made it quite slow. Therefore, this method has only been applied to one single (section of a) turn to provide a result showing the concept. The standard situation as described in section 3.8 is used with the robot modelled in the TS. In Figure 39 the result is to be observed. The figure shows the spatial pattern of the track with the distinction of the ITEs. For each area, the corresponding fBD was identified with the colours. From the graph, it is observed that for each track there is one main area to be identified where the peak compaction was observed (dark red).

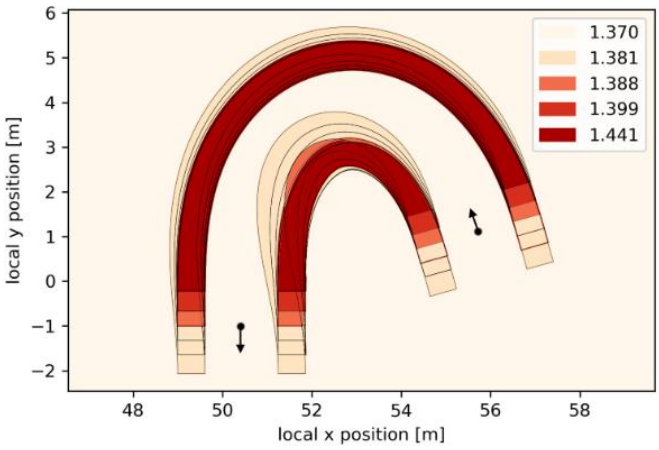

Figure 39: Representation of the spatial soil-track interactions where the legend shows the resulting bulk density values corresponding to the individual areas. The arrows indicate the driving direction.

5 Discussion

5.1 The Soil Model

The soil model and its adaptations have provided a way to calculate compaction. The results seem to be feasible, however, no validation of the results was possible as no data were available. To support the implementation of the SoilFlex model for tracked vehicles field tests are to be performed where the simulated results are to be compared with the findings in the field. As this is currently missing the presented results can only be interpreted as an approximation of the actual stress and change in BD in terms of the numeric results. Considering the stress patterns (Figure 22) in terms of their shape they do correspond with the findings of Keller and Arvidsson (2016).

The *stressTrackedTraffic* module provides a stress matrix for different depths. However, the compaction at different depths is not specifically analysed. Meaning that the influence of cultivation operations at certain depths was not covered. One example where the compaction at given depth levels would be of interest is that the compaction is mainly observed in the upper soil layers. This means that in the case of certain cultivation practices, the compaction might even be completely removed because of this operation. The remedy for improving the compacted soil is to plough or perform a subsoiling operation that sufficiently loosens up the soil. These operations are however costly in terms of fuel consumption. Considering the alternative no-till cultivation systems it is found that the soil will build a structure where the effects of compaction are degrading and the yield is not influenced (soilhealthpartnership, 2020). Approaching both possibilities, the corresponding aspects do introduce new implications. For given operations the compaction aspect might be of less interest compared to others and how are these differences in interest measured?

Nevertheless, soil compaction is an important topic in agriculture. As Shaheb et al. (2021) describes in their literature review that the secondary cost introduced by compaction in the form of increased energy use, accelerated wear on equipment, and the risk of recompaction all indicate a strategic way of farming is necessary to minimize soil compaction.

5.2 Soil-Track Interactions

5.2.1 Bulk Density

Considering the results, the approach of splitting the ITEs showed to provide useful insights related to the change in Bulk Density resulting from the passing of the track. The created patterns provide insights into what happens below the soil surface due to the trafficking of a tracked vehicle. Especially, the patterns introduced by the different vehicle states (Figure 25) can explain the differences in the compaction on headlands compared to the resulting soil compaction in the inner field. In the process, a similar method has been implemented as is done in alternative research which provided outcomes with are in line with the findings in this project (Amsing, 2021).

For the determination of the load on the individual ITEs, three variations of a load distribution have been implemented. These load distributions were substantiated approximations based on the underlying concepts suggested by alternative research. However, this still means that the used distributions were assumed to be correct. However, based on information on the vehicle it should be possible to extract the actual exact values for the loads on the ITEs. These values could be retrieved by doing a physical analysis on the robot or systematically finding the pressures on the ITEs using weigh cells. Doing this for both the OS and the TS makes the generation of results more accurate and better representative of the real situation.

The models used for calculating the compaction required inputs related to the soil state and variables. The analysis of a predefined situation as is done in this project makes the implementation of the model relatively simple. In practice, however, insight into soil state of the whole field is required to accurately simulate the introduced compaction for the whole field. This implies spatial data regarding the soil state is required. This, however, is not per se an easy task. Variability with fields can be relatively large (pdok, 2022) and the moisture content needs to be measured. This requires multiple precision farming solutions. The technology to provide this information does exist and by making use of weather stations this might be possible. However, this high level of data acquisition is not common practice in the Dutch arable agricultural sector yet (Kempenaar, 2020). This aspect will probably decrease the adoptability and implementation of the compaction aspect in practice.

The results of this research provided the fBD after the passing of a track system (Figure 25). The direct relation of these values considering plant growth restrictions is not considered. It is expected that a more compacted soil (higher fBD) will limit the possibility for roots to penetrate the soil resulting in growth restrictions. Considering literature on this topic it was found that actual implications related to the growth restrictions were identified but these are crop-specific (Houlbrooke et al., 1997; Lipiec et al., 2003; Tokunaga, 2006; Unger & Kaspar, 1994).

The methodology makes it possible to link the bulk density results with the spatial patterns. This has been the reason for the approach using ITEs. The question is if this is necessary as in Figure 39 it was observed that the peak compaction takes place in one specific area per track. This means there could be alternative implementations that are able to calculate this fBD based on the full track instead of considering the ITEs. The benefit of such an alternative approach is the simplification which initiates a decrease in the computational requirement. Especially for the F2C project, where such a methodology is to be implemented, it is important to consider these types of possible simplifications.

5.2.2 Disturbed Area

The current way of calculating the DA is relatively cumbersome. By representing the track by its 6 ITEs a total of 6 paths (Figure 26) and areas (Figure 27) will be calculated which were eventually combined (e.g Figure 32). This was done considering the idea of combining the spatial pattern with the bulk density. However, for only analysing the DA this method is to be simplified to improve the computational requirement. Only using the four corner points for creating the area feature below the track will already give enough insight by extruding this shape along the path relative to the COR. However, it is to be seen if this method is fast enough for implementation in F2C (Mier et al., 2023).

For the analysis of individual turns (section 4.3), there has been an argument based on peer feedback, that the total DA calculated is providing a high estimation of the DA of the actual turn. The reason for this is that the robot arrives at and leaves this turn. This means that part of the track is still on the inner part of the field when the turn is initiated or finished. It was suggested that the area considered for the straight swaths overlapping with the turning area should be compensated for. This means half of the total area of the tracks ($2*1/2*A_{track}$) should be deducted from the total DA of the turn. This compensation does apply when the direction of the field border is perpendicular to the working direction. However, this is not always the case as other angles were observed more commonly in the results. This makes the calculation of this correction more intricate than expected. Additionally, this correction only suffices when individual turns are compared, for a field scale analysis this correction does not apply, and every generated turn has a similar deviation related to this additional area. Therefore, it was argued that for only comparing turns, the proposed correction is not necessary to significantly improve the results.

The current implementation of the methodology uses an integration over the length of the path to determine the DA, this would imply that if the length is optimized, the compaction is already considered. This means that the models currently made do not add value in terms of optimization but

solely allow for insight based on the quantifications. To investigate this relationship the generated data was used to check the data for correlation in terms of the length of the path and the DA. The result (Figure 40) led to believe that the DA and the length of the turn are highly correlated as R^2 values ranging from 0.988 to 0.998 were found. This suggests that what was stated earlier as well, that when the length of a turn is minimized, the DA is also minimized, is therefore very plausible. This was explained by the methodology which uses the path as a primary input.

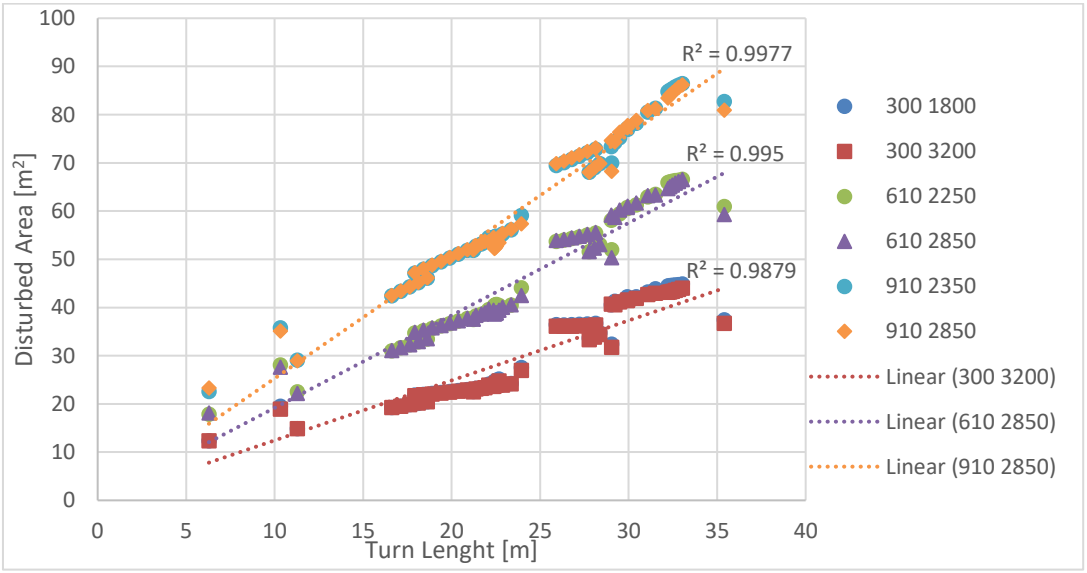

Figure 40: Graph showing the correlation between the turn length and the disturbed area for the results considering different track configurations ("300 1800" to be read as tread width and track width in millimetres).

One of the important aspects of this research was to research the variation of turning operations. In the methodology, the paths generated only contained Dubins and Reeds-Shepp curves. However, many alternatives are possible as described in the research by Sabelhaus et al. (2013). The Dubins variation results in omega- or U-turns. However, suiting to different situations, e.g. the minimal longitudinal width turn, for minimizing the width of the headlands could be of interest when no headlands are used, alternative turning options could result in better adaptability for the final generated solution to match the requirements set by farmers for creating the implicit paths for the robot.

5.3 Model Sensitivity

Related to the SA for the compaction it was found that, in case of this project, the soil type is one of the major input variables influencing the outcomes (Figure 30). Sandy soils show to be more prone to compaction which can be substantiated by the bigger pore spaces due to the larger particles which will be compressed more easily (Howell, 1997). However, the influence on crop growth is less critical on sandy soils compared to clay soils. This is the result of the difference in the ease of removing compaction on sandy soils. The removal of compaction is easier on sandy soils whereas clay soils have more long terms problems when soil is compacted (Warren & Taylor, 2017).

For the relation with the iBD and the fBD a linear relation was found (section 4.3, Figure 30), however, it was expected that for higher BDs the effect would decline as the soil is already compacted partly. In literature, it was found this relation of that BD is dependent on the water contents of the soil (Nawaz et al., 2013). As this relation has not been researched concerning the applied model, it is suspected that the critical water content level is not reached in the simulated examples and therefore the expected decrease in the data was not observed (Fratta & Kim, 2015; Haseeb, 2017).

The DA was found to be correlated with the length of the path (Figure 40). This makes that a comparison to alternative research was made on the path length and turning variations. In this case the

results in the paper by Sabelhaus et al. (2013) were used. The main aspect that is compared here is the shape of the observed patterns considering the change in the same input variable. In the paper by Sabelhaus et al. (2013), tests were performed on the longitude and lateral offsets for the start and end points of turns. Considering the patterns, a similar shape was identified substantiating the findings that there is an optimal working width and longitudinal offset concerning the set turning radius.

5.4 Field analysis

The current generation of turns provides unrealistic results in specific cases. The application of Reeds-Shepp turns on a field scale resulted in generated solutions that were not suitable for the application in practice. The reason for this is that the turning operation was performed mainly in the inner field (Figure 35). An alternative approach is needed to perform an accurate analysis of the Reeds-Shepp turning variation. Extending the straight swaths such that the turning operation takes place on the headlands would be the suggested solution. The length of this required offset can be determined by moving the turn DA pattern in the direction of the swath till the DA is not intersecting with the inner field anymore. This would preserve the original and optimized inner field pattern and does not alter the path currently calculated for the turning operation. Another problem faced with the generated turns was the introduction of circular patterns using the continuous curvature variation of the Dubins turn.

For the field analysis, the result of driving the set route is that in the end the inner field is completely cultivated. In practice, the next step would be to perform the cultivation on the headlands. Considering the results, it is found that the start and end positions based on the inner field operation do not have a good position for continuing the headland operation. It is expected that having these positions randomly assigned, as it is now, will cause additional compaction and DA (Spekken, 2010). Therefore, it is suggested to implement a cost related to these positions in the optimization. Here the distance to the starting position of the headlands and the field approaches needs to be considered.

In the implementation of a generated path in practice, it is important to consider the cultivation of the crop. The objective does vary based on the crop. An example would be to minimize compaction in the cultivation of cereal crops as these crops can gain higher yields when the soil structure is more suitable (Passioura, 1991). Additionally, it is preferred to cultivate the whole field to maximize the potential of the whole area. Alternatively, in the cultivation of onions or potatoes where beds or ridges are used, the goal is to maximize the area of the beds and ridges (Kouwenhoven, 1978). This is to be related to the minimization of the DA. In this section, it becomes clear that the practical implementation of a generated solution will be a key aspect for farmers to adopt autonomous solutions.

Speaking of the implementation in practice there is also a rise of interest in alternative cultivation systems. In the Netherlands, strip cultivation is being researched and alternatively controlled traffic farming (CTF) is considered in multiple parts of the world. As a foray into these ideas, a few solutions on a field scale were generated using the CTF approach. It is found that the DA can be reduced significantly. This does, however, mean that the areas where the tracks have driven are prone to higher compaction, and this area is not used for the cultivation of crops. However, the expected higher yield should compensate for this loss in the cultivated area (Antille et al., 2019; Hefner et al., 2019).

5.5 In-Situ Test

For the most accurate DA results, in relation to reality, the generated path is to be followed exactly. However, deviations from this path due to the field conditions or false settings can introduce undesirable effects. From practical experience, it is found that these effects are likely to occur. Therefore, the simulated results will not perfectly represent what will happen in the field. You always cope with irregularities within the field which the guidance system is susceptible for and tries to compensate for (Sharma et al., 2016). However, these guidance systems do have limitations causing deviation in the set and actual path.

6 Conclusion and Recommendations

In this research topics related to the interaction between the tracks of a UGV and the soil have been investigated through literature research, the introduction and implementation of new methods, and eventually the application of these methods generating the results. This has also involved the application of the F2C library for the generation of path data. In this process, the research questions introduced in section 1.5, have formed the lead in this project. In this chapter, the answers and findings related to these questions are provided considering the results and discussion.

6.1 What model is suitable for predicting soil compaction created by a tracked vehicle?

In the process of performing this research, the decision of using the SoilFlex model employing the SoilPhysics library was made early on to provide the opportunity the explore the possibilities of this model. This led to testing the original library and secondly, the suitability of the model was tested. It was found that the original library could be implemented to provide an approximation of the real situation but in the original form, the model did not specifically suit tracked vehicles. Through a literature search, a paper was found providing alternative equations which allowed for modifying the model to better suit a tracked vehicle. With this modification, the resulting stress patterns met the expected shape as was originally described. Considering the results, it was found that this modified SoilFlex model provided feasible and useful results for the simulation and prediction of soil compaction for a tracked vehicle. The validation of the outcomes of the model are not part of this research. The reason for this is that implementation of the model for a tracked vehicle comes back little in alternative research and it does not allow for a fair comparison. Experiments for tracked vehicles within the field could provide this information. It is of great value to perform tests in a wide variety of situations to gain insight into the robustness of the current state of the model.

6.2 What manoeuvring aspects of a track-driven vehicle are to be considered for improving the generation of turns and how can these be quantified?

This question refers to the quantification of the processes occurring during the execution of a turning operation. The determination of the physical influence on the soil is researched and additionally, the spatial situation is investigated by means of the covered area by the tracks of the AgXeed Agbot 5.115T2. This has resulted in two quantified aspects. The compaction, in terms of the (change in) bulk density [Mg/m^3] and the disturbed area [m^2]. This is done utilizing the physical properties (dimensions and weight) of the robot and the implements. Additionally, two states have been defined accounting for the robot during the cultivation or the turning operation. The approach in this project was based on the analysis of ITEs. These are the idlers and rollers of the track. For the determination of the load on the individual ITEs, three variations of a load distribution were implemented. These load distributions were substantiated approximations based on the underlying concepts suggested by alternative research.

Related to the spatial manoeuvring aspects of the AgBot the disturbed area was introduced to quantify the skidding of the tracks during turns. The Fields2Cover software library was used for the generation of the paths. These paths were used for the approximation of the local contact area, called the disturbed area, by the robot. Initially, the focus has been on the turns, and in a later stage, full field analysis was added. Setting up the methodology it was found that the results were dependent on the location of the centre of rotation (COR) of the robot. This location is approximated in this project, it is suggested to create a tool for determining this location based on the robot-implement setup.

6.3 Which model variables incite a sensitive response concerning the compaction and disturbed area quantifications?

Through a sensitivity analysis, the influence of the input variables on the models was researched. This analysis focussed on the compaction and the disturbed area. For the compaction model it was found that, related to the soil, the initial bulk density plays a major role the in the final bulk density. A linear relationship was found opposing the expected relation which was that a more compacted soil would be less prone to additional compaction.

Considering the physical aspects of the robot in terms of size and its configuration it was found that the tread width has a significant influence on both the compaction model and the outcome of the disturbed area quantification. The relation is however discrapent to each other. To decrease the disturbed area, it is preferred to have a narrower track. This does however result in higher compaction rates. So, related to these aspects the cultivation practices are to be considered.

Concerning the generation of the paths the turn radius is to be minimized to reduce the disturbed area. However, a smaller turn radius results in more skidding. This is substantiated by the field test where the patterns were captured by means of images captured by a drone. Considering this it was found that in terms of the swaths, the lateral offset has a big influence. This relates to the working width of the implement. It has been found that based on the turning radius there is an optimal working width which makes that the required path for the turning operation can be optimized in terms of length and the DA.

Related to the turn types the standard versions (so not the continuous curvature variations) of the Dubins and Reeds-Shepp variation provides the best results. The problem with this turn types is that instantaneous turning is required (rotating at a fixed position). This leads to the degradation of the top layer of the soil. This opposes the goal of minimizing soil impact as a central concept in the report. In this project, it was found that the Dubins with continuous curvature show the most realistic curves in terms of implementation in reality and is therefore the preferred method. Alternative solutions are to be implemented to see how relevant these are in terms of practical implementation.

6.4 Which of the currently implemented turns produces the least disturbed area comparing a selection of generated paths based on a convex agricultural field with an arbitrary shape using the AgXeed AgBot 5.115T2?

In the results, it was found that the total area, in terms of the number of square metres, does not always tell the full story. It is important to analyse the results visually to determine the possible application in practice. Considering the generated results for this project for the test field. The situation where the direction was based on the optimization for the total length, a snake swathing order, and the boustrophedon turn type was implemented resulted in the best situation considering the DA. In this case, a total area of 3046.90 m^2 of the total 10,000 m^2 of the field was required for the cultivation of the inner part of the field. The second-best solution was optimized for the number of swaths and used a spiral pattern (n=4). Where a total DA of 3078.58 m^2 was necessary to cultivate the whole field. This shows that there are combinations of settings that result in an optimal solution related to the measured aspect.

The final aspect to think about is the cultivation system implemented. In this projec, the cultivation system was considered as a standard cultivation system. Alternatives like controlled traffic farming (CTF) where out of the scope of this project. However, some testing on CTF situations indicated that this system provides a promising alternative. Considering some generated output a reduction of about 63-66% in terms of the DA can be achieved by introducing CTF. Therefore, it is recommended to consider the implementation of CTF more prominently in the continuation of the F2C project.

7 References

AgXeed. (n.d.-a). AgBot 5.115T2. Retrieved November 9th, 2022 from https://www.agxeed.com/our-solutions/agbot-5-115t2/

AgXeed. (n.d.-b). AgXeed webpage. Retrieved September 7th, 2022 from https://www.agxeed.com/

Akca, A., Kara, I., & Aydos, M. (2020). *Privacy, Security and Legal Aspects of Autonomous Vehicles*. Retrieved from IMSMATEC'20: https://www.researchgate.net/publication/343376262_Privacy_Security_and_Legal_Aspects_of_Autonomous_Vehicles

AMAZONE. (n.d.-a). Cenius mounted cultivator. Retrieved Februari 8th, 2023 from https://amazone.net/en/products-digital-solutions/agricultural-technology/cultivation/cultivators/anbaugrubber-cenius-53238

AMAZONE. (n.d.-b). Gedragen cultivator Cenius & Getrokken cultivator Cenius-2TX. Retrieved Januari 19th, 2023 from https://info.amazone.de/DisplayInfo.aspx?id=69684

Amsing, L. (2021). *Route Optimisation Reducing Soil Compaction in Agricultural Operations*. Retrieved from supervisor (dr.ir. S de Bruin)

Antille, D., Peets, s., Galambošová, J., Botta, G. F., Rataj, V., Macak, M., . . . Godwin, R. (2019). Review: Soil compaction and controlled traffic farming in arable and grass cropping systems. *Agronomy Research, 17*, 653-682. doi:10.15159/AR.19.133

Brase, T. (2005). *Precision Agriculture*: Delmar Cengage Learning.

Buckman, H. O., & Brady, N. C. (1960). *The nature and properties of soils* (6th ed.).

CHN Industrial. (2017). Autonomous tractor technology shows way forward for farming: enhancing efficiency and working conditions in agriculture. Retrieved September 7th, 2022 from https://media.cnhindustrial.com/emea/CASE-IH/autonomous-tractor-technology-shows-way-forward-for-farming--enhancing-efficiency-and-working-condit/s/d9d11785-2881-4577-afc2-23e6dadbfc91

Clemson University. (n.d.). GPS Guidance Basics. Retrieved September 12th, 2022 from https://www.clemson.edu/extension/agronomy/PrecisionAgriculture/docs/GPS_Basics.html

Cuaran, J., & Leon, J. (2021). Crop Monitoring using Unmanned Aerial Vehicles: A Review. *Agricultural Reviews, 42(2)*, 121-132. doi:10.18805/ag.R-180

de Bruin, S. (2020). Fields2cover: Robust and efficient coverage paths for autonomous agricultural vehicles. Retrieved September 6th, 2022 from https://www.wur.nl/en/project/Fields2cover-Robust-and-efficient-coverage-paths-for-autonomous-agricultural-vehicles.htm

de Bruin, S. (2022). [Personal Communication].

de Lima, R. P., da Silva, A. P., Giarola, N. F. B., da Silva, A. R., Rolim, M. M., & Keller, T. (2018). Impact of initial bulk density and matric suction on compressive properties of two Oxisols under no-till. *Soil and Tillage Research, 175*, 168-177. doi:10.1016/j.still.2017.09.003

de Lima, R. P., & da Silva, A. R. (2021a). soilDeformation.R. Retrieved November 7th, 2022 from https://github.com/arsilva87/soilphysics/blob/master/R/soilDeformation.R

de Lima, R. P., & da Silva, A. R. (2021b). stressTraffic.R. Retrieved November 7th, 2022 from https://github.com/arsilva87/soilphysics/blob/master/R/stressTraffic.R

de Lima, R. P., da Silva, A. R., & da Silva, Á. P. (2021). Soilphysics: An R package for simulation of soil compaction induced by agricultural field traffic. *Soil and Tillage Research, 206*, 104824. doi:10.1016/j.still.2020.104824

de Lima, R. P., Rolim, M. M., C. Dantas, D. d., da Silva, A. R., & Mendonça, E. A. S. (2021). Compressive properties and least limiting water range of plough layer and plough pan in sugarcane fields. *Soil Use and Management, 37*(3), 533-544. doi:10.1111/sum.12601

Defossez, P., & Richard, G. (2002). Models of soil compaction due to traffic and their evaluation. *Soil and Tillage Research, 67*(1), 41-64. doi:10.1016/S0167-1987(02)00030-2

Ding, Z., Munkholm, L. J., ten Damme, L., & Lamandé, M. (2022). Vertical and horizontal soil stresses beneath a modern combine harvester: Measurements and modelling. *Land Degradation and Development, 33*(6), 892-903. doi:10.1002/ldr.4191

Dobretsov, R. Y., Sokolova, V. A., Teterina, I. A., Malyukov, S. V., Aksenov, A. A., & Smertin, N. V. (2021). Interaction feature of caterpillar tracks with soil under significant axial displacements of pressure center. *IOP Conference Series: Earth and Environmental Science, 839*(5), 052023. doi:10.1088/1755-1315/839/5/052023

Dubins, L. E. (1957). On Curves of Minimal Length with a Constraint on Average Curvature, and with Prescribed Initial and Terminal Positions and Tangents. *American Journal of Mathematics, 79*(3), 497-516. doi:10.2307/2372560

ducksize.com. (n.d.). AgXeed Agbot. from https://nl.ducksize.com/product-page/agxeed-agbot

Dziuk, B. (2021). 5 Benefits of Farm GPS Tracking + What Today's Farmers Think About It. Retrieved November 9th, 2022 from https://info.rastrac.com/blog/farm-gps-tracking

ESRI. (n.d.). How Union works. Retrieved November 10th, 2022 from https://desktop.arcgis.com/en/arcmap/10.3/tools/analysis-toolbox/how-union-analysis-works.htm

European Commission. (2021). *EU agricultural outlook for markets, income and environment, 2021-2031*. Retrieved from

Fendt. (2020). Latest generation of seed sowing robots: The Fendt Xaver comes of age. Retrieved September 12th, 2022 from https://www.fendt.com/int/2-fendt-xaver

Fendt. (n.d.-a). Fendt VarioGuide Contour Assistant and adaptive Curve. Retrieved September 12th, 2022 from https://www.fendt.com/us/smart-farming/varioguide

Fendt. (n.d.-b). Project Xaver: Research in the field of agricultural robotics. Retrieved September 8th, 2022 from https://www.fendt.com/int/xaver

Fields2Cover. (2022a). Part 3: Headland Generator - Constant Width Headland. Retrieved September 12th, 2022 from https://fields2cover.github.io/source/tutorials/python_headland_generator.html

Fields2Cover. (2022b). Part 4: Swath Generator. Retrieved September 12th, 2022 from https://fields2cover.github.io/source/tutorials/python_swath_generator.html

Fields2Cover. (2022c). Part 5: Route Planning - Snake Order. Retrieved September 12th, 2022 from https://fields2cover.github.io/source/tutorials/python_route_planning.html

Fields2Cover. (2022d). Part 6: Path planning - Dubins curves with Continuous curvature. Retrieved September 9th, 2022 from https://fields2cover.github.io/source/tutorials/python_path_planning.html#

Fratta, D., & Kim, K.-S. (2015). *Effective Depth of Soil Compaction in Relation to Applied Compactive Energy*. Retrieved from https://wisconsindot.gov/documents2/research/WisDOT-WHRP-project-0092-08-11-final-report.pdf

H-Wodka. (n.d.). Protocol voor het inmeten van brutoperceel. from https://docplayer.nl/9294078-Protocol-voor-het-inmeten-van-brutoperceel.html

Haseeb, J. (2017). Compaction of Soil - Uses and Effects of Soil Compaction. Retrieved Februari 28th, 2023 from https://www.aboutcivil.org/compaction-of-soil-uses-and-effects.html

Hefner, M., Labouriau, R., Nørremark, M., & Kristensen, H. L. (2019). Controlled traffic farming increased crop yield, root growth, and nitrogen supply at two organic vegetable farms. *Soil and Tillage Research, 191*, 117-130. doi:10.1016/j.still.2019.03.011

Houlbrooke, D. J., Thom, E. R., Chapman, R., & McLay, C. D. A. (1997). A study of the effects of soil bulk density on root and shoot growth of different ryegrass lines. *New Zealand Journal of Agricultural Research, 40*(4), 429-435. doi:10.1080/00288233.1997.9513265

Howell, J. (1997). Soil Basics Part I: Physical Properites of Soil. from https://ag.umass.edu/vegetable/fact-sheets/soil-basics-part-i-physical-properites-of-

soil#:~:text=Sandy%20soils%20have%20rather%20large,pore%20space%20than%20sandy%20soils.
International Labour Organization. (2021). Employment in agriculture (% of total employment) (modeled ILO estimate. Retrieved October 11th, 2022 from https://data.worldbank.org/indicator/SL.AGR.EMPL.ZS
John Deere. (2022). John Deere Reveals Fully Autonomous Tractor at CES 2022. Retrieved September 8th, 2022 from https://www.deere.com/en/news/all-news/autonomous-tractor-reveal/
Keller, T. (2005). A Model for the prediction of the contact area and the distribution of vertical stress below agricultural tyres from readily available tyre parameters. *Biosystems Engineering, 92*(1), 85-96. doi:10.1016/j.biosystemseng.2005.05.012
Keller, T., & Arvidsson, J. (2007). Compressive properties of some Swedish and Danish structured agricultural soils measured in uniaxial compression tests. *European Journal of Soil Science, 58*(6), 1373-1381. doi:10.1111/j.1365-2389.2007.00944.x
Keller, T., & Arvidsson, J. (2016). A model for prediction of vertical stress distribution near the soil surface below rubber-tracked undercarriage systems fitted on agricultural vehicles. *Soil and Tillage Research, 155*, 116-123. doi:10.1016/j.still.2015.07.014
Keller, T., Défossez, P., Weisskopf, P., Arvidsson, J., & Richard, G. (2007). SoilFlex: A model for prediction of soil stresses and soil compaction due to agricultural field traffic including a synthesis of analytical approaches. *Soil and Tillage Research, 93*(2), 391-411. doi:10.1016/j.still.2006.05.012
Kempenaar, C. (2020). Precision farming on Dutch arable farms: status, challenges and outlook. Retrieved March 1th, 2023 from https://www.agroberichtenbuitenland.nl/binaries/agroberichtenbuitenland/documenten/publicaties/2020/07/09/corne-kempenaar-farminar-presentation/Corne+Kempenaar+Farminar+presentation+July+8%2C+2020.pdf
Kharel, T. P., Ashworth, A. J., Shew, A., Popp, M. P., & Owens, P. R. (2020). Tractor guidance improves production efficiency by reducing overlaps and gaps. *Agricultural & Environmental Letters, 5*(1), e20012. doi:10.1002/ael2.20012
Kouwenhoven, J. (1978). Ridge quality and potato growth. *Netherlands Journal of Agricultural Science, 26*(3), 288-303.
Kramer, H., Mucher, S., Franke, G. J., Kooistra, L., Suomalainen, J., & Bartholomeus, H. (2015). Meer detail met UAV's. *Geo-Info, 12*(2), 34-36. Retrieved from https://edepot.wur.nl/430398
LaValle, S. M. (2020a). 15.3.1 Dubins Curves. Retrieved September 13th, 2022 from http://lavalle.pl/planning/node821.html
LaValle, S. M. (2020b). 15.3.2 Reeds-Shepp Curves. Retrieved September 13th, 2022 from http://lavalle.pl/planning/node822.html
Li, Q., Ayers, P. D., & Anderson, A. B. (2007). Modeling of terrain impact caused by tracked vehicles. *Journal of Terramechanics, 44*(6), 395-410. doi:10.1016/j.jterra.2007.09.001
Lipiec, J., Medvedev, V., Birkas, M., Dumitru, E., Lyndina, T., Rousseva, S., & Fulajtar, E. (2003). Effect of soil compaction on root growth and crop yield in Central and Eastern Europe. *International agrophysics, 17*(2). Retrieved from http://www.international-agrophysics.org/pdf-106728-37570?filename=Effect%20of%20soil%20compaction.pdf
Liu, W., & Cheng, K. (2020). An Analytical Model for Predicting Ground Pressure under a Rigid-Flexible Tracked Vehicle on Soft Ground. *Mathematical Problems in Engineering, 2020*. doi:10.1155/2020/6734121
Liu, W., Cheng, K., & Wang, J. (2018). Failure analysis of the rubber track of a tracked transporter. *Advances in Mechanical Engineering, 10*(7). doi:10.1177/1687814018789526
Mier, G. (2022). Fields2Cover. Retrieved September 9th, 2022 from https://fields2cover.github.io/index.html

Mier, G., Valente, J., & de Bruin, S. (2023). *Optimizing agricultural coverage path to minimize soil compaction*. Paper presented at the ECPA2023.

Naio Technologies. (n.d.). OZ, The Farming Assistant for Time-Consuming and Arduous Tasks. Retrieved September 9th, 2022 from https://www.naio-technologies.com/en/oz/

Nawaz, M. F., Bourrié, G., & Trolard, F. (2013). Soil compaction impact and modelling. A review. *Agronomy for Sustainable Development, 33*(2), 291-309. doi:10.1007/s13593-011-0071-8

Nielsen, L., Sung, I., & Nielsen, P. (2019). Convex Decomposition for a Coverage Path Planning for Autonomous Vehicles: Interior Extension of Edges. *Sensors, 19*, 4165. doi:10.3390/s19194165

NPPL. (2019). Variabel kunstmest strooien grasland werkt in de praktijk. Retrieved September 8th, 2022 from https://www.proeftuinprecisielandbouw.nl/variabel-kunstmest-strooien-grasland-werkt-in-de-praktijk/

O'Sullivan, M., Henshall, J., & Dickson, J. (1999). A simplified method for estimating soil compaction. *Soil and Tillage Research, 49*(4), 325-335.

O'Sullivan, M. F., & Robertson, E. A. G. (1996). Critical state parameters from intact samples of two agricultural topsoils. *Soil and Tillage Research, 39*(3-4), 161-173. doi:10.1016/S0167-1987(96)01068-9

Passioura, J. (1991). Soil structure and plant growth. *Soil Research, 29*(6), 717-728.

pdok. (2022). Dataset: Basisregistratie Ondergrond (BRO). Retrieved March 1th, 2023 from https://www.pdok.nl/introductie/-/article/basisregistratie-ondergrond-bro-

Python. (n.d). from https://www.python.org/

r2py. (n.d.). R in python. from https://rpy2.github.io/

R. (n.d.). The R Project for Statistical Computing. from https://www.r-project.org/

Reeds, J. A., & Shepp, L. A. (1990). OPTIMAL PATHS FOR A CAR THAT GOES BOTH FORWARDS AND BACKWARDS. *Pacific Journal of Mathematics, 145*, 367-393.

Rehman, A., Jingdong, L., Khatoon, R., Hussain, I., & Iqbal, M. S. (2016). Modern agricultural technology adoption its importance, role and usage for the improvement of agriculture. *Life Science Journal, 14*(2), 70-74. Retrieved from http://www.lifesciencesite.com/lsj/life140217/10_29837lsj140217_70_74.pdf

Sabelhaus, D., Röben, F., Meyer zu Helligen, L. P., & Schulze Lammers, P. (2013). Using continuous-curvature paths to generate feasible headland turn manoeuvres. *Biosystems Engineering, 116*(4), 399-409. doi:10.1016/j.biosystemseng.2013.08.012

Saxton, K. E., & Rawls, W. J. (2006). Soil water characteristic estimates by texture and organic matter for hydrologic solutions. *Soil Science Society of America Journal, 70*(5), 1569-1578. doi:10.2136/sssaj2005.0117

Shaheb, M. R., Venkatesh, R., & Shearer, S. A. (2021). A Review on the Effect of Soil Compaction and its Management for Sustainable Crop Production. *Journal of Biosystems Engineering, 46*(4), 417-439. doi:10.1007/s42853-021-00117-7

Shamshiri, R., Weltzien, C., Hameed, I. A., J Yule, I., E Grift, T., Balasundram, S. K., . . . Chowdhary, G. (2018). Research and development in agricultural robotics: A perspective of digital farming.

Shapely. (n.d.). Shapely. Retrieved November 10th, 2022 from https://github.com/shapely/shapely

Sharma, K. R., Honc, D., & Dusek, F. (2016). *Predictive Control Of Differential Drive Mobile Robot Considering Dynamics And Kinematics.* Paper presented at the European Conference on Modelling and Simulation.

Söhne, W. (1953). Druckverteilung im Boden and Bodenverformung unter Schlepperreifen. Landwirtschaft und Umwelt.(Pressure distribution in soil and soil deformation under tractor tyres). *Agriculture and environment. Landtechnik, 5*, 49-63. doi:10.1007/BF01512930

soilhealthpartnership. (2020). Transitioning to no-till. Retrieved Februari 28th, 2023 from http://www.soilhealthpartnership.org/wp-content/uploads/2020/08/SHP-info-no-till-2020.pdf

Spekken, M. (2010). *Optimizing Routes on Agricultural Fields Minimizing Maneuvering and Servicing Time*. Retrieved from https://edepot.wur.nl/173653

Teimourlou, R., & Taghavifar, H. (2015). Determination of the Super-Elliptic Shape of Tire-Soil Contact Area Using Image Processing Method. *Cercetari Agronomice in Moldova, 48*. doi:10.1515/cerce-2015-0026

Tokunaga, A. (2006). Effects of bulk density and soil strength on the growth of blue wildrye (Elymus glaucus Buckl.).

Tsouros, D., Bibi, S., & Sarigiannidis, P. (2019). A Review on UAV-Based Applications for Precision Agriculture. *Information, 10*, 349. doi:10.3390/info10110349

U.S. Department of Agriculture. (2022). Farm Labor. Retrieved October 12th, 2022 from https://www.ers.usda.gov/topics/farm-economy/farm-labor/

Unger, P. W., & Kaspar, T. C. (1994). Soil Compaction and Root Growth: A Review. *Agronomy Journal, 86*(5), 759-766. doi:10.2134/agronj1994.00021962008600050004x

Van den Akker, J. (2004). SOCOMO: a soil compaction model to calculate soil stresses and the subsoil carrying capacity. *Soil and Tillage Research, 79*(1), 113-127. doi:https://doi.org/10.1016/j.still.2004.03.021

van der Horst, A. (2015). Bewaren 2.0. Retrieved October 12th, 2022 from https://edepot.wur.nl/356505

Versluis, H. (2006). Bewaarcomputer neemt werk uit handen. *Landbouwmechanisatie : vakblad voor akkerbouwers, veehouders en loonwerkers 57 (10): 24 - 25*. Retrieved from https://edepot.wur.nl/7046

Warren, J., & Taylor, R. (2017). Managing Soil Compaction. Retrieved Februari 28th, 2023 from https://extension.okstate.edu/fact-sheets/managing-soil-compaction.html

Wong, J. Y., & Huang, W. (2008). Approaches to improving the mobility of military tracked vehicles on soft terrain. *International Journal of Heavy Vehicle Systems, 15*(2-4), 127-151. doi:10.1504/IJHVS.2008.022239

Wong, J. Y., Jayakumar, P., & Preston-Thomas, J. (2019). Evaluation of the computer simulation model NTVPM for assessing military tracked vehicle cross-country mobility. *Proceedings of the Institution of Mechanical Engineers, Part D: Journal of Automobile Engineering, 233*(5), 1194-1213. doi:10.1177/0954407018765504

Yakoubi, M. A., & Laskri, M. T. (2016). The path planning of cleaner robot for coverage region using Genetic Algorithms. *Journal of Innovation in Digital Ecosystems, 3*. doi:10.1016/j.jides.2016.05.004

8 Appendices

Appendix A. Contents of the .zip file and folder structure

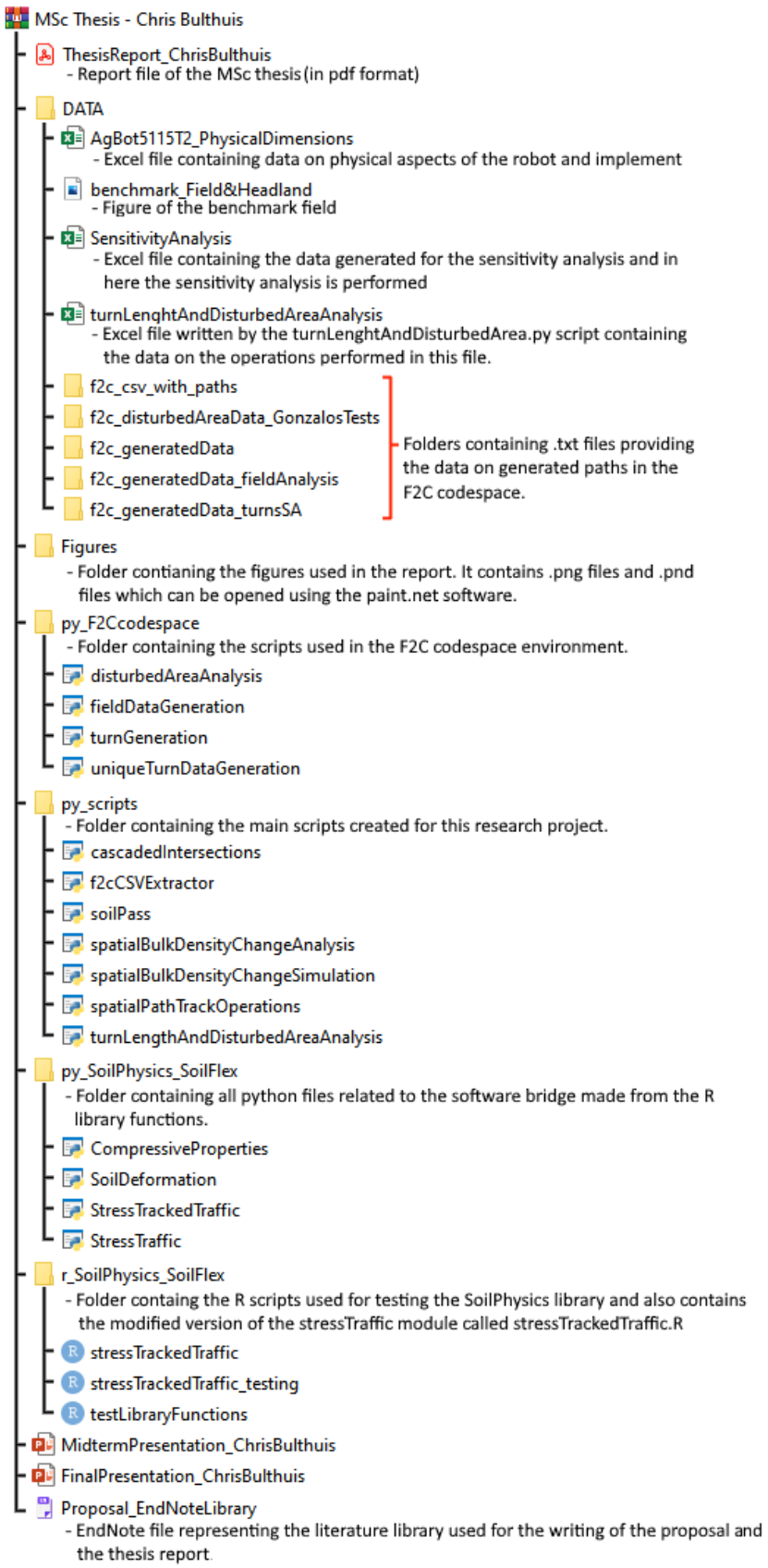

Appendix B. AgBot5115T2_idlerAndRollerDimensions.xlsx
Excel file containing the numeric values of the dimensions used in this report. This file can be found in the .zip file in the DATA folder.

Appendix C. Physical dimensions of the AgBot 5.115T2. Retrieved from: (AgXeed, n.d.-a)

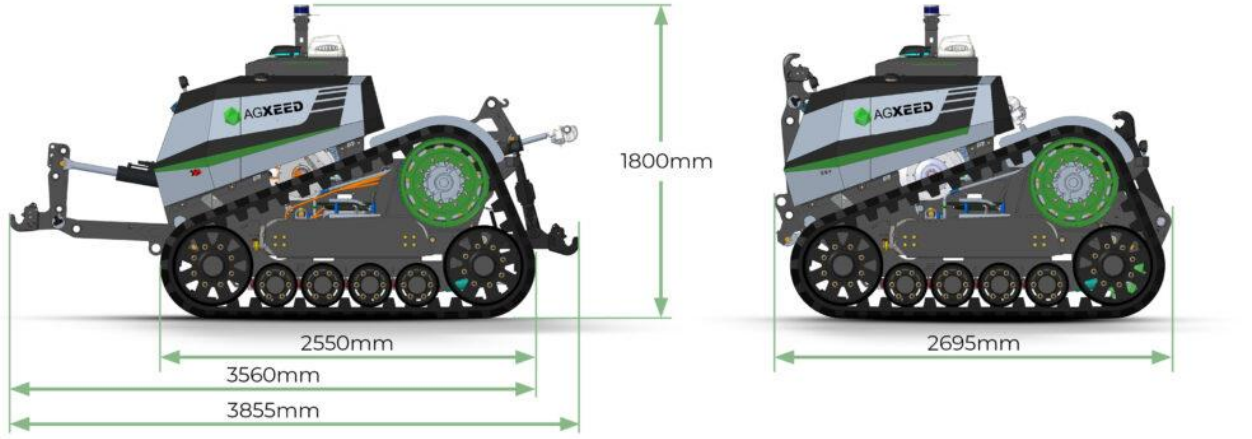

Appendix D. Overview of the available track widths per track type for the AgBot 5.115T2. The configuration used in this project is indicated with the red dashed square. Retrieved and modified from: (AgXeed, n.d.-a).

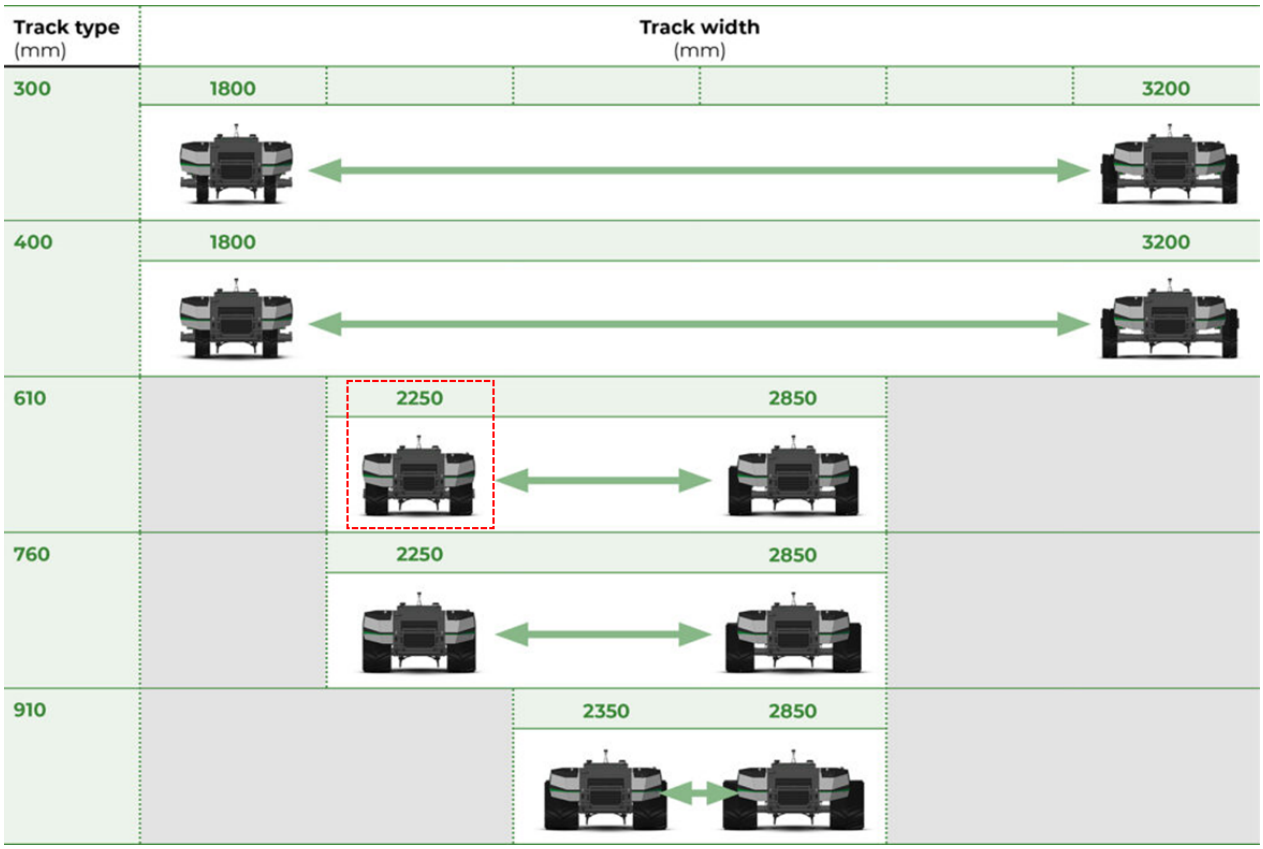

Appendix E. Graphical substantiation of how, based on the coordinates (x,y) of the centre of rotation of a tracked vehicle, the position of an individual track element can be calculated using the known parameters values of the angle of direction (α), the track width (TW) and the distance of the centre of rotation to the track element (COR_{offset}).

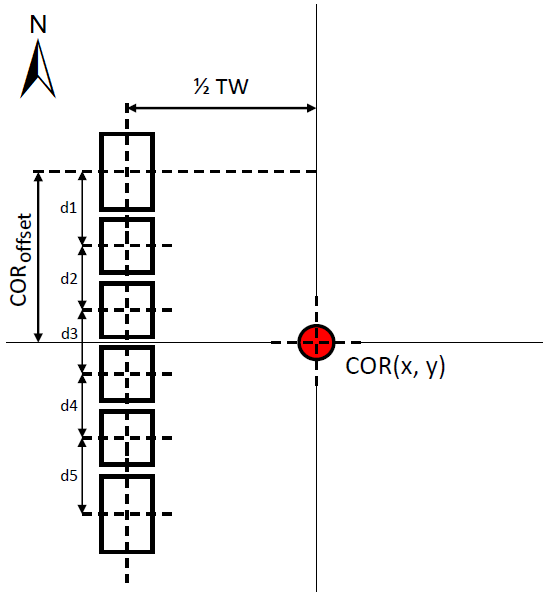

Definition of Principal Elements and Distances

Top-down view of the track indicating the individual elements. COR(x,y) is the centre of mass of the robot. The distance between the COR(x,y) and the centre of the track is represented by ½TW (half of the track width). COR_{offset} represents the distance from the first track element to the COR(x,y). Lastly, d1…d5 represent the distances between the individual elements. The implementation in code uses the distances as represented in Figure 17

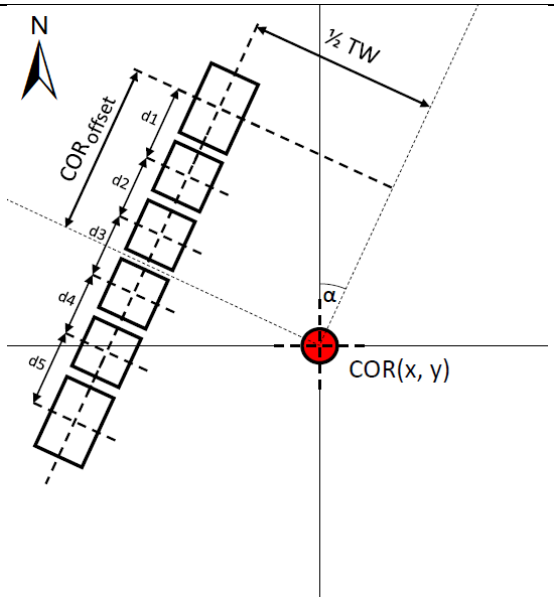

Introduce Rotation

By introducing an angle, the resulting positions of the track elements change.

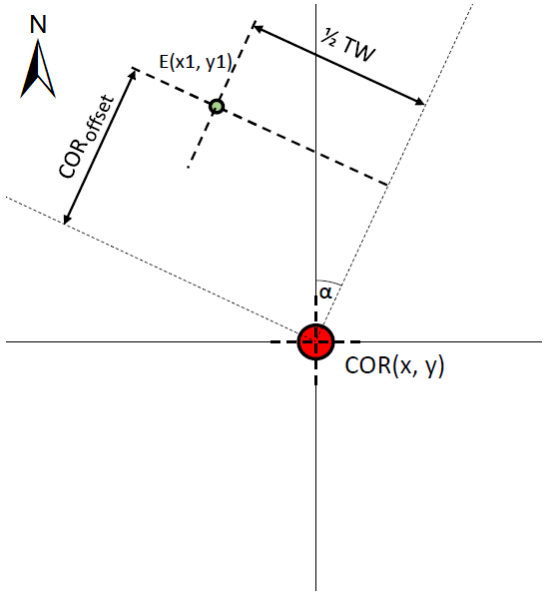

Single Track Element

The goal is to find the relation between COR(x,y) and the individual track element (E) which allows to calculate x1 and y1 based given the position of COR(x,y).

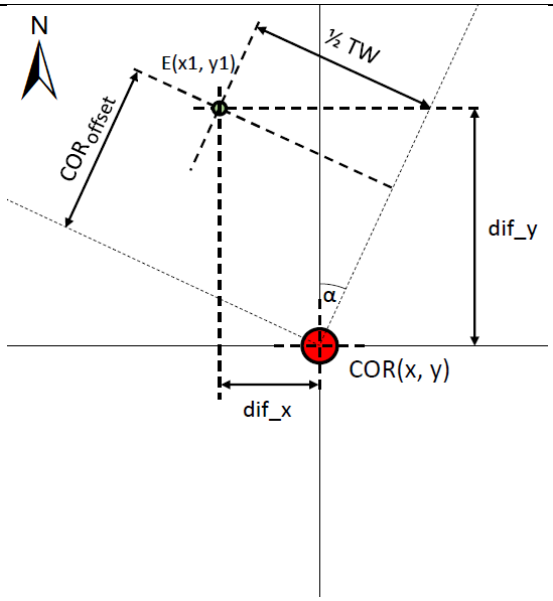

Required Offsets

The required offsets to transform x to x1 and y to y1 are defined as dif_x and dif_y.

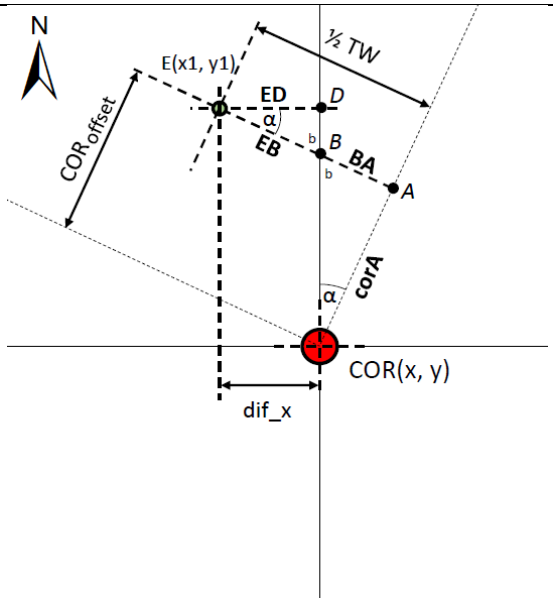

Calculation of x1

Based on the properties of a triangle it is found that triangle CORAB (α, b and A∟ = 180°) and EBC (α, b and C∟ = 180°) are uniform triangles.

$$corA = COR_{offset}$$

$$BA = \tan(\alpha) * corA$$

$$EB = 1/2TW - BA$$

$$ED = \cos(\alpha) * EB$$

$$dif_x = ED$$

$$x1 = x - dif_x$$

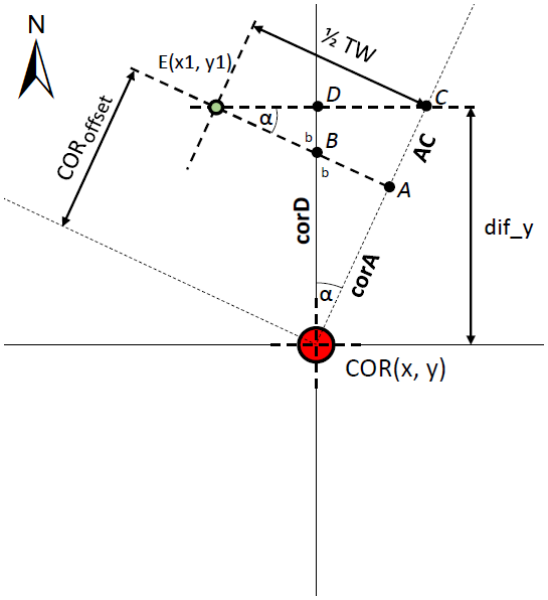

Calculation of y1

Based on the properties of a triangle it is found that triangle CORAB (α, b and A∟ = 180°), EAC (α, b and A∟ = 180°) and CORDC (a, D∟, b_c = 180°) are uniform triangles.

$$corA = COR_{offset}$$

$$AC = \tan(\alpha) * 1/2TW$$

$$comD = \cos(\alpha) * (corA + AC)$$

$$dif_y = corD$$

$$y1 = y + dif_y$$

Appendix F. Code for generating the convex field and headland.

```
import fields2cover as f2c              # imports the library
rand = f2c.Random(42)                   # defines the seed for the random operator
robot = f2c.Robot(2.0, 3.0)             # defines physical width and working width of the robot
constant_hl = f2c.HG_Const_gen()
field = rand.generateRandField(5, 1e4) # generates a random field of 1e4 m² with 5 sides.
cells = field.field
no_hl = constant_hl.generateHeadlands(cells, 12) # generates the inner part of the field
                                                   defining the headland border
```

Appendix G. Disturbed Width analysis on the turns identified in Figure 27

Turn 1

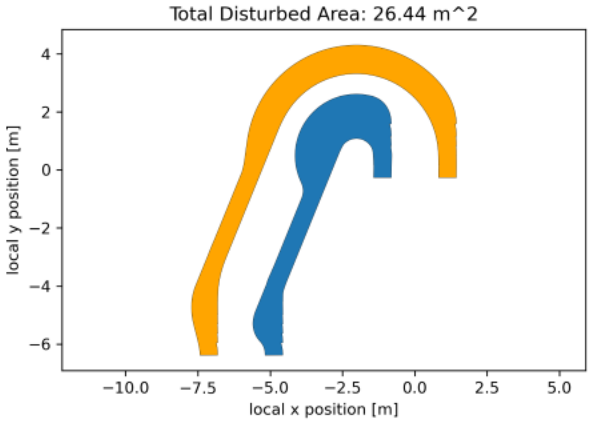

Turn 2

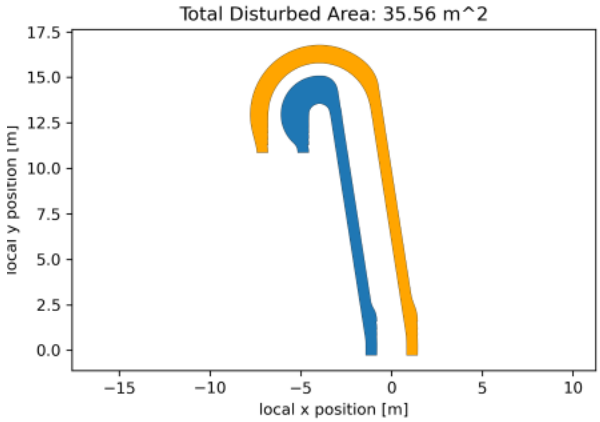

Turn 3

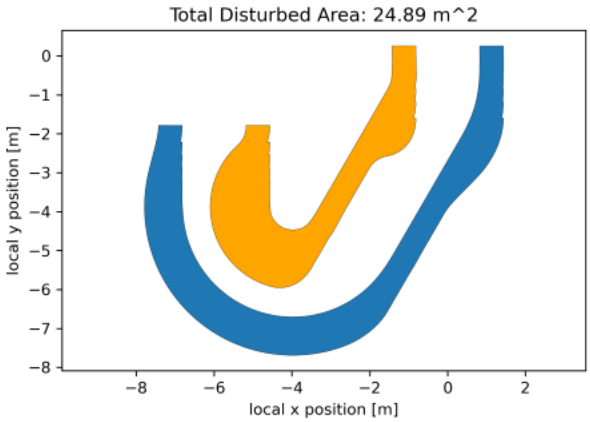

Turn 4

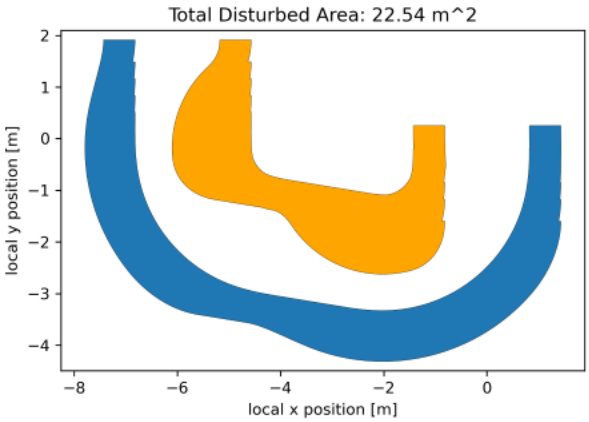

Turn 5

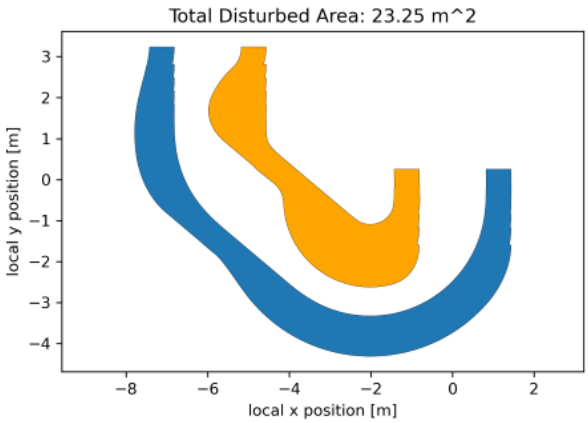

Turn 6

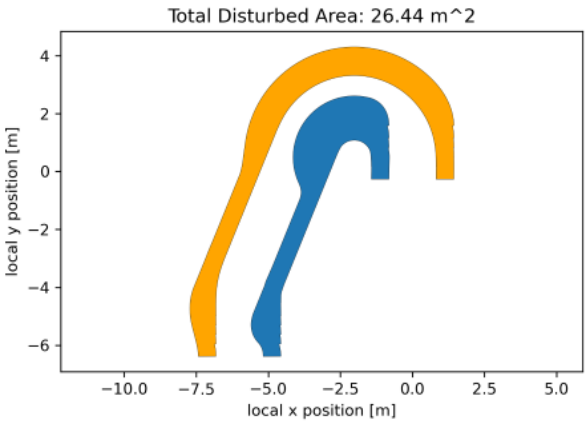

Appendix H. SensitivityAnalysis.xlsx

This excel file can be found in the .zip file of the deliverables and contains the data and results used for the execution of the Sensitivity Analysis.

Appendix I. Sensitivity Analysis Graph of the Bulk Density for the Operating State. The Tread Width and iBD are quantitative variables and the others are qualitative variables. Load Distribution: 0 – Custom, 1 – Uniform, 2 – Triangular. Soil Type: 0 – Sandy Clay Loam, 1- Sandy Loam. Soil State: 0 – Wet, 1 – Dry.

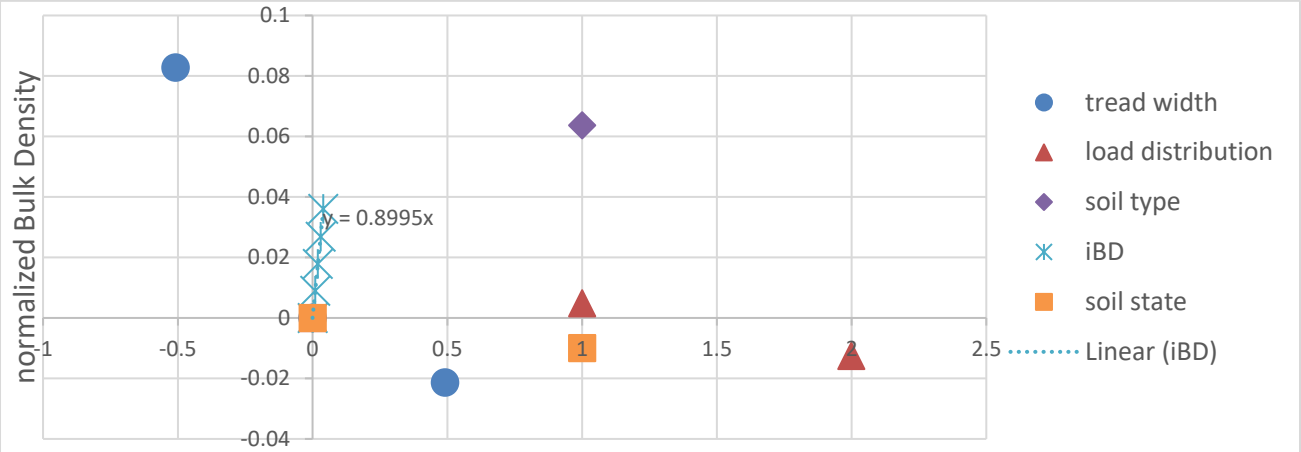

Appendix J. Sensitivity Analysis Graph of the Disturbed Area.

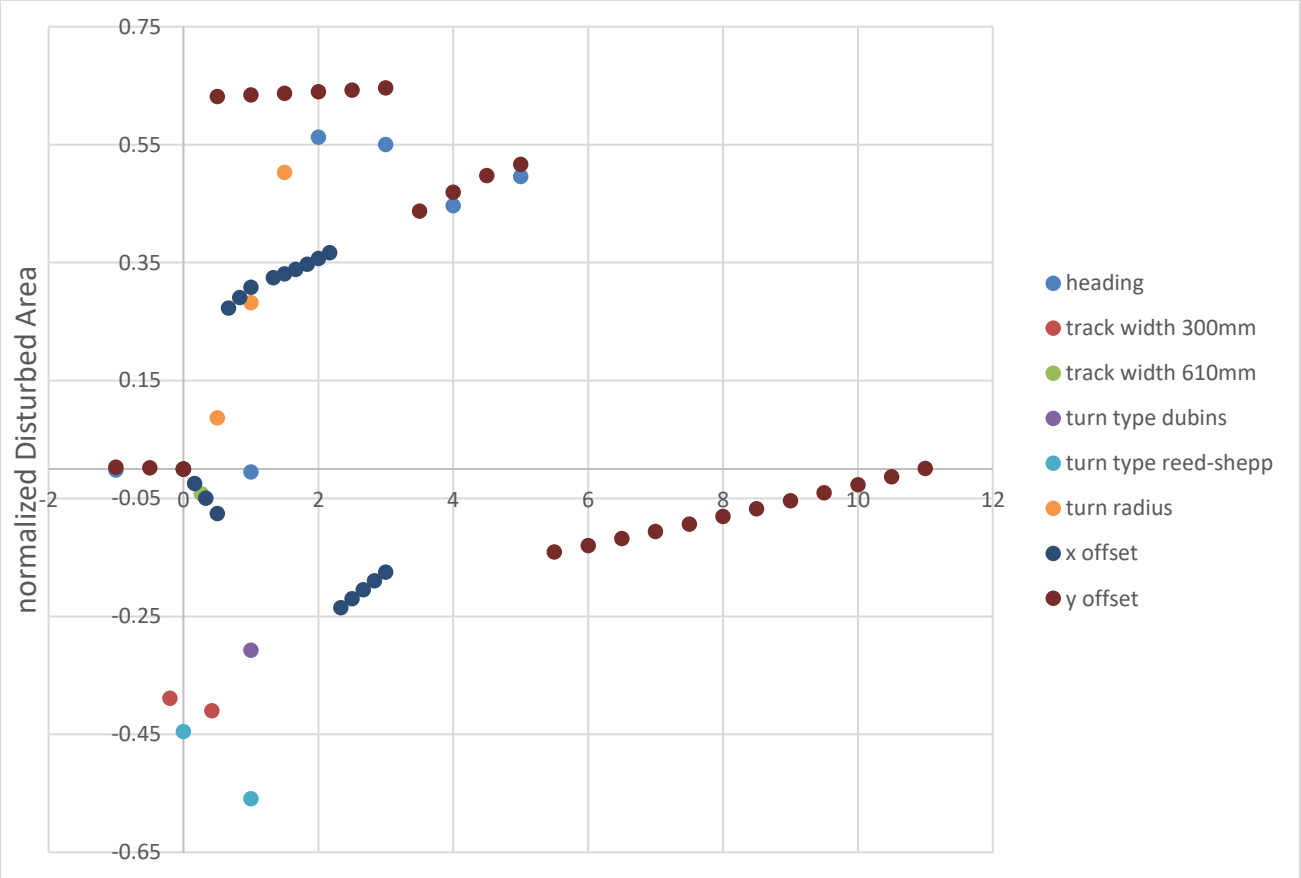

Appendix K. Figures Representing Disturbed Area Patterns Generated for the Results on Field Scale.

Pattern 5

Reeds-Shepp

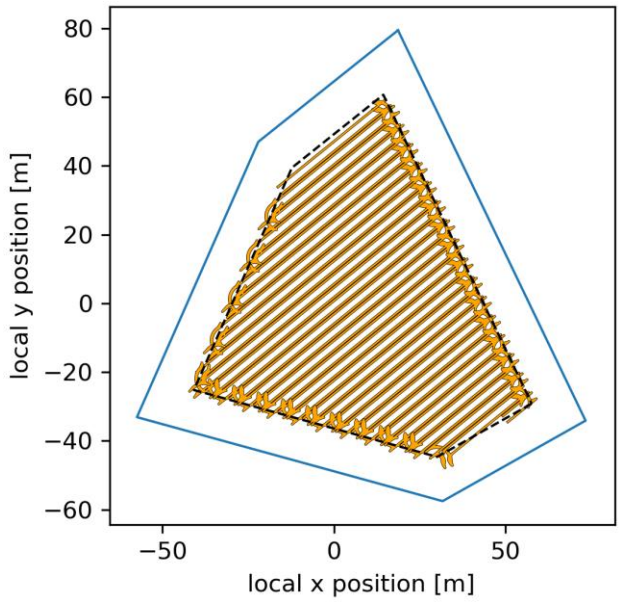

Pattern 7

Optimized for the number of Swaths with a snake ordering pattern.

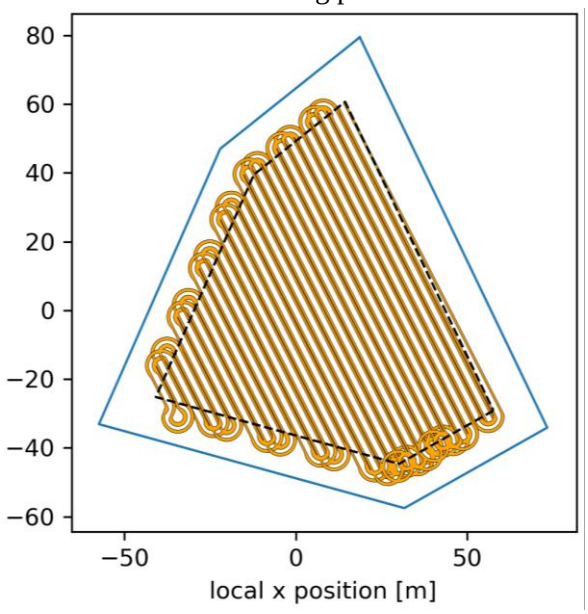

Pattern 9

Optimized for the number of Swaths with a spiral ordering pattern where n is set to 4 swaths.